Department of Geology
Institute of Earth Sciences
The Hebrew University of Jerusalem

Multi-scale aeromagnetic UAV based survey for detecting magmatic and tectonic features: A case study from the Hula Valley, Dead Sea Fault

Thesis for Degree of Master of Science
Submitted by

Eldar Buzaglo-Yoresh

Under the supervision of:

Prof. Amotz Agnon[1]
Dr. Bruno Gavazzi[2]

December 2022
כסלו התשפ״ג

1.Neev Center for Geoinfomatics, Fredy & Nadine Herrmann Institute of Earth Sciences, the Hebrew University of Jerusalem, Jerusalem, 91904, Israel

2. ENEREX, Nancy, France

Acknowledgements

First and foremost, I would like to dedicate this thesis to the late Professor Marc Munschy. Marc opened the doors to the world of magnetism for me and taught me with endless patience and great humor. Also, he inherited the scripts for the processing and interpretation software AppliMag.

I thank Professor Amotz Agnon for enlightening ideas and guidance for the Nebi Huda site and the past surveys. His advice, diligence, and precision in science and language will lead me wherever I turn.

Thank you to Dr. Bruno Gavazzi for close and quality scientific support and teaching. Also, an extensive amount of mental help was just as significant.

Dr. John Hall for his support of the Niv Center and the students active in it. Also, I thank you very much for the best and fastest proofreading I could ask for and, of course, for the guidance under the accompanying committee.

To Professor Ron Shaar for his membership in the accompanying committee and guidance under an introductory course to Paleomagnetism, in which the final project included measurements that contributed to the thesis.

To TERRALOG INNOVATIONS for the days of surveying and processing the data.

Many thanks to my father, Avi Buzaglo-Yoresh, for the professional, personal, and everything in-between help.

Also, thanks to my classmates who helped a lot, each in their way:

Adar Glazer, Erez Hassul, Yaniv Darvasi, and Amir Joffe.

and last as first,

Thanks to Tamar, my beloved wife.

And thanks to my family:

Inbal, Avi, Arad, and Neomi.

Abstract

This study focuses on the transition zone between the Hula Valley and the slopes of the Golan Heights, straddling the ‘Azaz fault. The geological features are not known at a precise local scale due to sediment coverage on the Hula side and complex extrusion-erosion history of the Golan side.

Following technological advances in recent years, drones are used for near-surface airborne magnetic surveys, filling the gap between aircraft-based and ground-based surveys. This work presents an innovative multi-scale aeromagnetic study for exploring the geological characteristics in the Nebi-Huda vicinity at the Golan foothills in the eastern Hula Valley.

The survey is based on the geological map of Mor (1987), Mount Odem. We chose to focus on the Nebi-Huda site due to the exposure of several interesting geological types, with unknown protractions with depth in the basin. The main and most prominent is the ‘Azaz fault, a secondary branch of the boundary between the Arabian and African plates. Southeast of ‘Azaz, two additional minor faults crop out on the Golan Heights.

The fault shifts the Hula block left-laterally relatively to the Golan Heights (on the Arabian plate). The fault also uplifts the cover basalt, including the Ein-Zivan basalt, on the east. The latter flowed in a ravine incised in the former, opposite the Hula-filling in the west. East of ‘Azaz Fault, the massive Ein-Zivan basalt flowed down an ancient channel (part of it still drains a runoff) and “disappears” where it meets the fault.

The sensor was first flown at a height of 100m above ground level (AGL) to obtain a preliminary map of the magnetic field in the area and have an overview of the main geological features. In the second stage, the area was mapped from a height of 50m AGL to get additional details of the magnetic anomalies. Finally, we focused on areas of interest derived from the published maps and flew over them at a low altitude of 25m AGL to obtain an increased resolution of identified magnetic anomalies.

The study results reveal a new NS limit interpreted as a buried fault system parallel to the ‘Azaz Fault on its west. Secondary contacts within the basin suggest a complex prism-shape stepping toward the basin. Also, the magnetic maps, combined with paleomagnetic data, allow a more detailed mapping of the basaltic flows under the sediment cover in the Nebi-Huda region.

סקר מגנטי-אווירי מבוסס רחפן ממספר גבהים לאיתור מאפיינים מגמתיים וטקטוניים:

מקרה בוחן מעמק החולה, העתק ים המלח

בעקבות התקדמויות טכנולוגית של השנים האחרונות, רחפנים משמשים לסקרים מגנטיים מוטסים קרובים לפני הקרקע, וממלאים את הפער בין סקרים מבוססי מטוסים לאלו הקרקעיים. עבודת מחקר זו מציגה סקר מגנטי חדשני מבוסס רחפן ממספר גבהים לחקר המאפיינים הגיאולוגיים בסביבת נבי-הודא במזרח עמק החולה.

הסקר מבוסס על המפה הגיאולוגית של מור (1987), הר אודם. בחרנו להתמקד באתר נבי-הודא מכיוון נחשפים מספר סוגים של מופעים גיאולוגיים מעניינים, אך התפוצה שלהם לעומק האגן אינה ידועה. העיקרי והבולט ביותר הוא העתק עזז, שהוא ענף משני של גבול הלוחות הערבי והאפריקאי. דרומית מזרחית לעזז במורדות הגולן נחשפים שני העתקי משנה.

ההעתק מסיט את גוש החולה לכיוון דרום ביחס לרמת הגולן (שהיא חלק מהלוח הערבי). ההעתק גם מעלה את בזלת הכיסוי, כולל בזלת עין-זיוון, ממזרח. האחרונה זרמה בגיא שנחרץ בבזלת הכיסוי, אל מול מילוי החולה במערב. ממזרח לעזז, בזלת עין-זיוון המסיבית זרמה במורד ערוץ עתיק (חלק ממנה עדיין מנקז מי נגר) ו"נעלמת" היכן שהשבר חוצה אותו.

החיישן הוטס בשלב ראשון בגובה של 100 מ' מעל פני השטח (מעפ"ש) כדי לקבל מפה ראשונית של השדה המגנטי באזור ולקבל סקירה של המאפיינים הגיאולוגיים העיקריים. בשלב השני מופה השטח מגובה 50 מ' מעפ"ש כדי לקבל פרטים נוספים על החריגות המגנטיות. לבסוף, התמקדנו באזורי עניין שנגזרו מהמפות הקיימות וטסנו מעליהם בגובה נמוך של 25 מ' מעפ"ש כדי להשיג רזולוציה מוגברת של חריגות מגנטיות שזוהו. את תוצאות הסקרים האוויריים בחנו אל מול שלושה סקרים מגנטיים קרקעיים. ובנוסף בחנו מדידות פליאוגמגנטיות שנאספו בשולי קילוח עין זיוון.

תוצאות המחקר חושפות אנומליה ארוכת גל הנפרשת בכיוון צפון דרום. את האנומליה אנו מייחסים להימצאות מערכת העתקים קבורה במקביל להעתק עזז. כמו כן, המפות המגנטיות בשילוב עם המדידות הפליאומגנטיות מאפשרות להציע מיפוי מפורט של הזרמים הבזלתיים מתחת לכיסוי המשקעים באזור נבי-הודא.

Table of Contents

1. Scientific background

1.1 Geological background

Separating the Sinai-Israel sub-plate from the Arabian plate, the Dead Sea Transform fault system (DST) forms a 1,000 km-long left-lateral lineament that runs between the northern reaches of the Red Sea Rift in the south to the East Anatolian Fault in the north (Fig. 1) (Freund et al., 1970). The DST was established as a plate boundary in the Early-Middle Miocene when strike-slip movement and normal faulting where initiated along its course (Nuriel et al., 2017). The geometry of the transform system, trending only slightly about N-S, is responsible for the formation of several basins (pull-aparts) and elevations (push-ups) as a result of local plate divergence or convergence along its route (e.g. Hula Basin (Garfunkel, 1981)). Such structures are being developed depending upon the orientation of the contact between the plates, relative to the vector of motion. The DST plate boundary is divided into three sectors: the southern and northern ones are controlled by stretched basins, whereas the central one is controlled by shortening and the formation of a mountainous area referred as the Lebanon restraining bend.

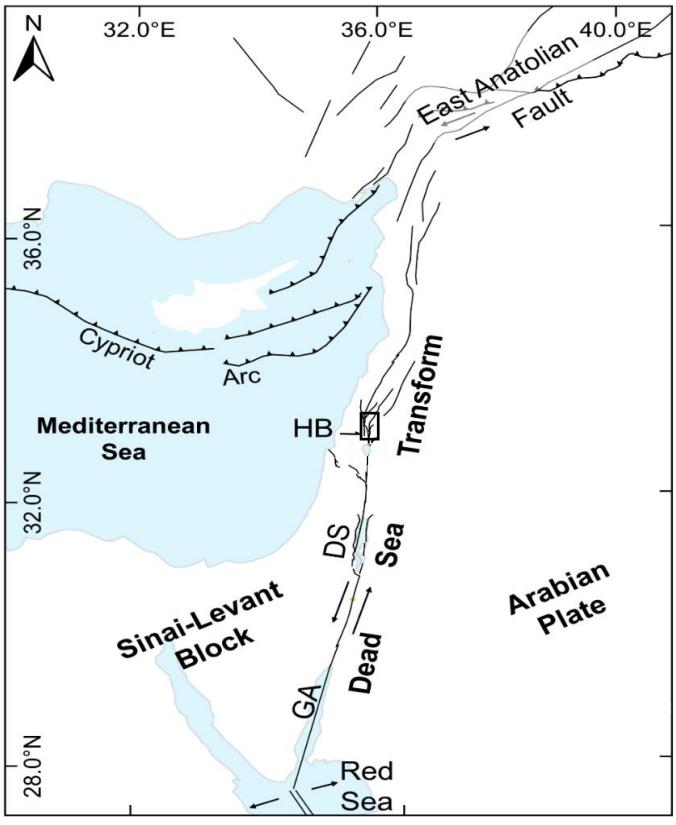

Figure 1 - Regional tectonic map of the Dead Sea transform system. Abbreviations: HB- Hula Basin; DS- Dead Sea; GA – Gulf of Aqaba (modified after Barnea Cohen et al., 2022).

The pre-transform architecture of the northern parts of the southern DST sector, including the Hula Valley and the Golan Heights (Fig. 2), is mainly controlled by Syrian Arc structures (synclines and anticlines) deforming marine carbonates of Jurassic to Eocene age (Garfunkel, 1981).

Geological and geophysical studies, as well as borehole investigations indicate that in the Hula Basin, the main DST splits into two sub- fault systems (Fig. 2) (Heimann et al., 1990; Rybakov et al., 2003; Politi & Agnon, 2009; Politi, 2011). The first, north and northwest of Hula, (i.e. the Yamuneh fault system) contains the Yamuneh and Roum faults. The other, to the northeast, includes the Rashaya-Serghaya pair of faults with a restraining step-over between them which uplifts Mount Hermon. This pair has generated significant seismic events in 1759 A.D. causing serious damage in Damascus and in numerous settlements in the Galilee, Golan, Lebanon and Palmyrides (Ambraseys, 1997).

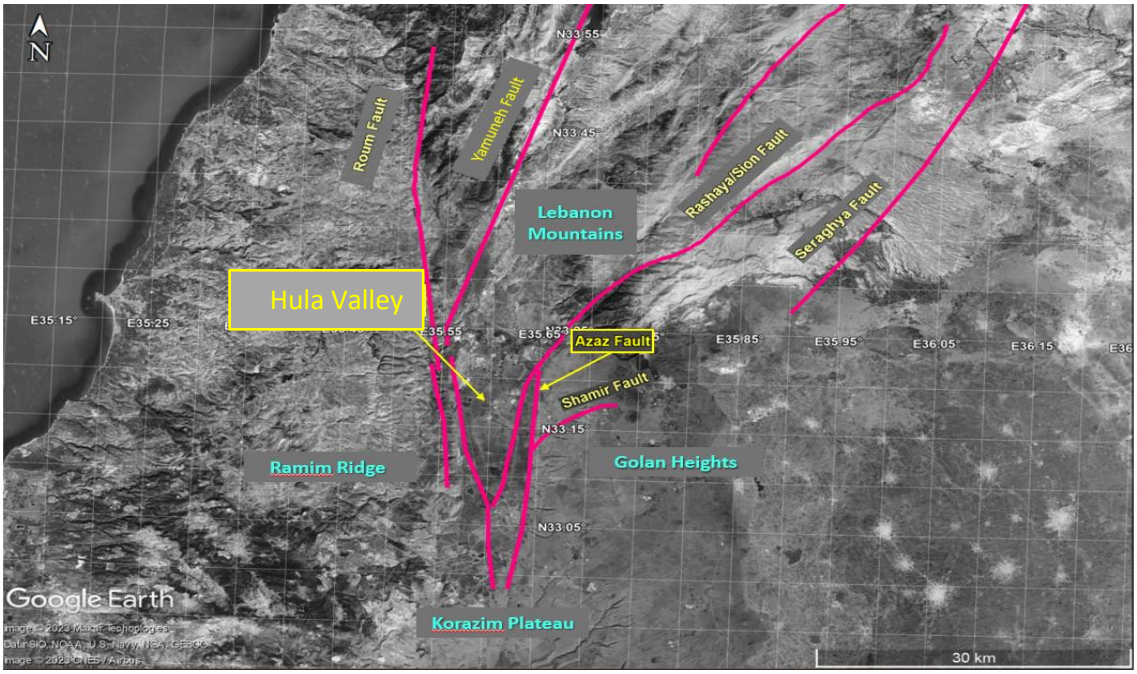

Figure 2 – The main fault systems in the northernmost part of the southern sector of the dead-sea fault (after Sneh & Weinberger,2004 and Politi,2011)

The Hula Valley formed as a pull apart sedimentary basin between the Yamuneh and the Rashaya-Serghaya fault systems, during the Early Pleistocene. The basin is about 22 km long and 7 km wide, located south of Lebanon's restraining mountains belt, east of the Ramim Ridge (a part of the Yamuneh Fault system), north of the Korazim

Plateau, and west of the Golan Heights (Fig. 2). The Rashaya Fault system, or by its local Hebrew name ‘Azaz Fault is the main fault of the northwestern margin of the basin (Fig. 2) (Heimann, 1990; Zilberman et al., 2000). The 'Azaz Fault consists of several right-stepping sections and forms a rhombic structure with a north-northeast strike and an 80 ° -85 ° dip (Heimann et al., 2009; Politi, 2011).

The western reaches of the Hula Basin are filled with a thick volcanic and sedimentary section. This section consists of a kilometer-thick basal layer of marl and pebbles (Heimann & Steinitz, 1989), covered by lacustrine carbonates and clastics interleaved with basalt flows and alluvial deposits (Fig.3)(Mor, 1993).

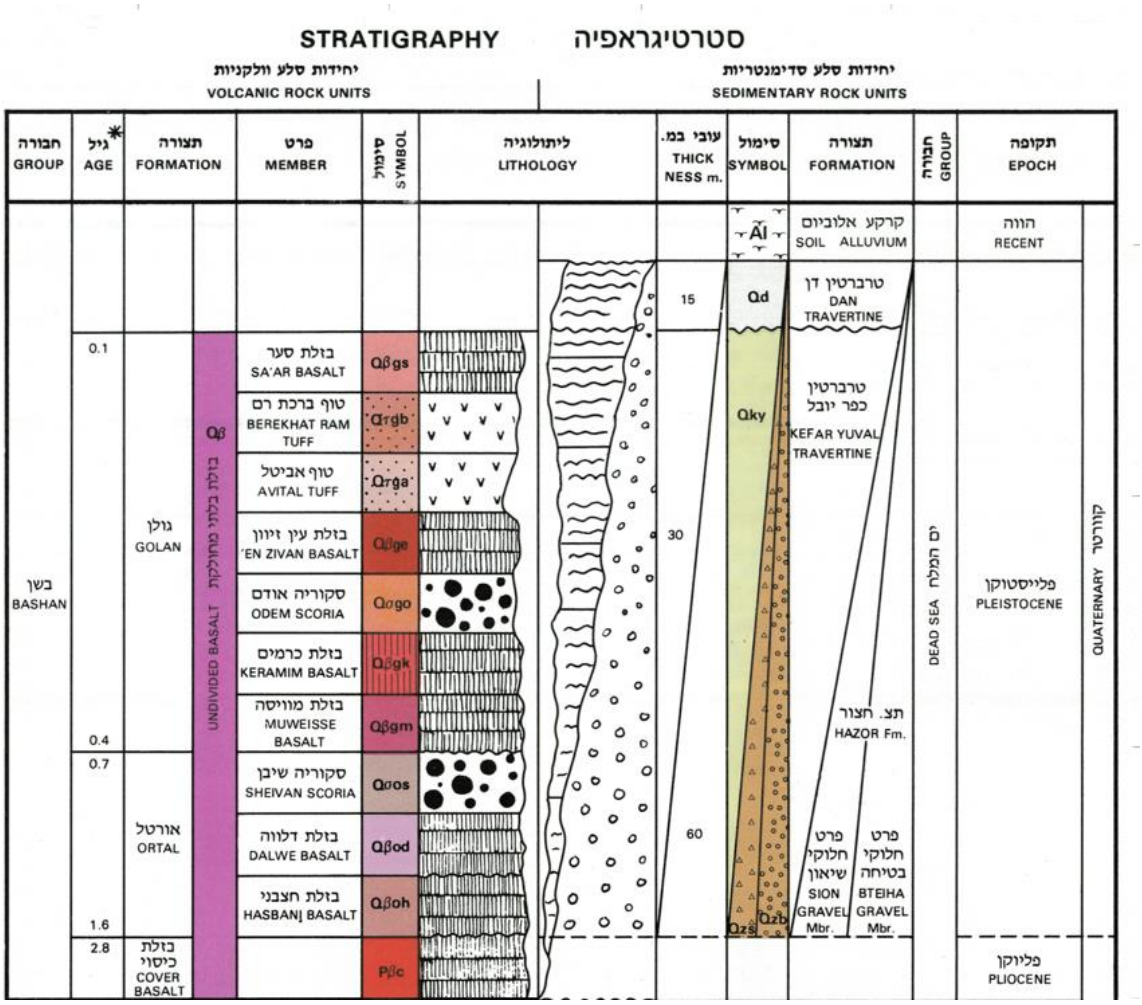

Figure 3 - Stratigraphic section of the units exposed in the western Hula Basin (Mor, 1987)

The ‘Azaz Fault separates the uplifted foothills of the Golan Heights to the east and the lowers Hula to the west. The Golan Heights span over 1300 Km^2 and reach an elevation of 2000m. This elevated area was initially formed due to extensive Plio-Pleistocene volcanic activity, including the eruption of significant volumes of basalt that filled the Syrian Arc syncline structure (Mor, 1993; Shaanan et al., 2011).

The Golan Heights area is bounded from north and south by the Hermon and Ajlun anticlines, respectively, and continues eastward into the Harrat – A(l)Sham volcanic field. To the west, the Golan Heights are interrupted by the Serghaya and Rashaya (‘Azaz / Sion) faults (Fig.2).

The base of the geological type section of the northwestern Golan Heights is composed mainly of Jurassic to Eocene carbonates of the Arad, Kurnub, Judea, Mount Scopus and Avedat Groups.

Since the Pliocene, extensive volcanic eruptions on the Golan Heights, have covered the older carbonate and clastic rocks. Volcanic rocks of the Plio-Pleistocene basaltic Bashan Group filled the Golan syncline, creating the first-order landscape elements we see today on the Golan Heights (Mor, 1986, 1993).

In this work, I will refer to ages determined using 40Ar/39Ar and K/Ar; however it is worth noting that dating based on argon isotopes alone is more reliable, and therefore, of greater weight. I will refer to potassium-argon dating only in cases where 40Ar/39Ar dates near the relevant site are unavailable. In general, the volcanic formations exposed in the Golan become younger northward (Behar et al., 2019). the Pliocene basalts range in age between 5.5 and 3.4 million years (Heimann, 1996), and the Pleistocene basalts 1.4 - 0.1 million years (Behar et al., 2019; Feraud et al., 1983; Shaanan et al., 2011; Tauxe et al., 2022).

The nature of the complex transition zone between the volcanics-dominated Golan Heights and the volcano-sedimentary Hula Basin is well-known at a regional scale. However, a detailed investigation of the partly exposed / partly buried contact along the 'Azaz Fault was needed as it was little studied. In the present study, an drone-based high resolution aeromagnetic survey around Nebi-Huda (Fig.4) intends to clarify

the nature of the mutual relationship between the basalt flows on the Golan slopes and their interaction with the sediment-filled basin.

1.2 The survey area

The study area extends between the foothills of the volcanic Golan Heights and the Hula Valley on both sides of the 'Azaz Fault. The area of the site is ca. 2 Km^2, with Nebi-Huda to the north and Givat-HaEm to the south (Fig. 4). The elevation difference is ~70m.

The Hula Quaternary section comprises 60m of mainly travertine and Kabul soil mixed with basaltic pebbles transported from the Golan Heights (Mor, 1993) (Fig. 4b).

The youngest basalts and the ones with the most extensive coverage in the working area are the basalts of the Golan Formation, which include the Muweisse and Ein Zivan basanite basalt flows (Shaanan et al., 2011; Weinstein et al., 2006). The latter, the youngest among them, is associated with the late Pleistocene period (0.1-0.4 Ma) (Heimann, 1990; Mor, 1993). The Ein Zivan basalt flow in the study area partially fills a gulley incised into older flows.

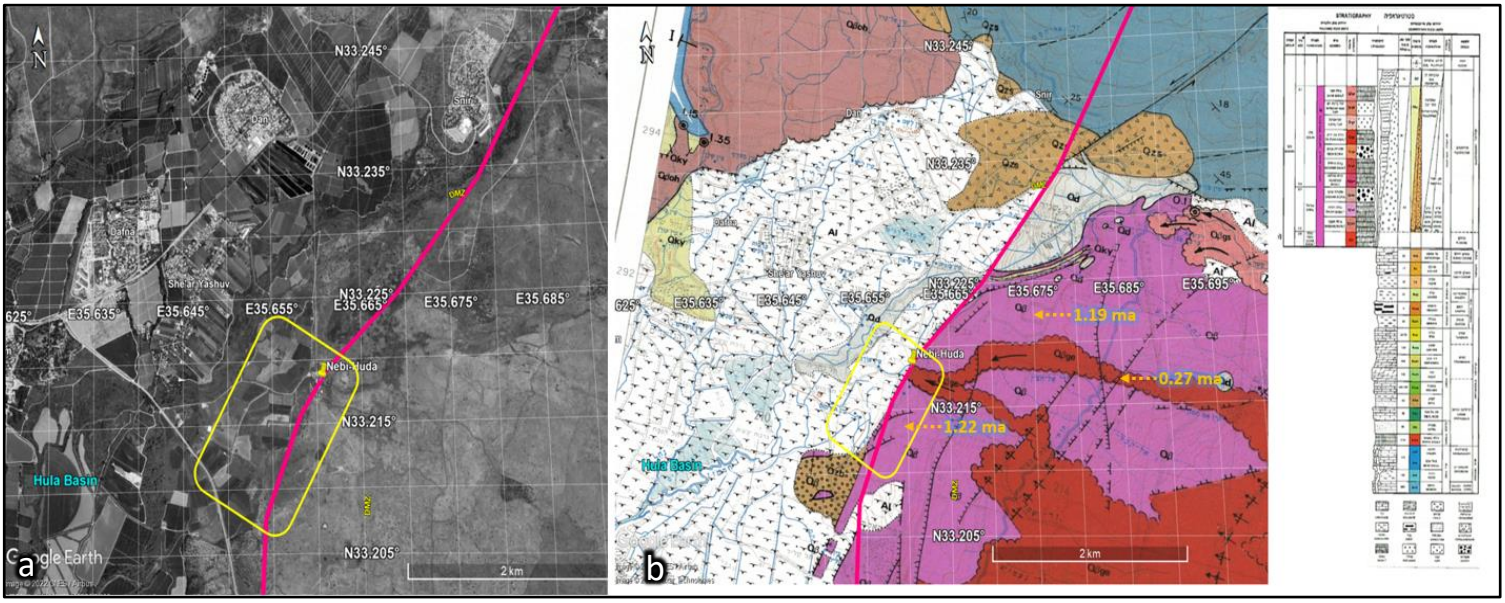

Figure 4 - (a) The Survey area marked in a yellow rectangle; (b) The survey area on top of a geological map of Mor, 1987, Ages based on Heimann (1990).

It propagated from east to west via an incision through undivided basalts of Late Pliocene age. The exposure terminates at the 'Azaz Fault trace near Nebi-Huda (Fig. 5b).

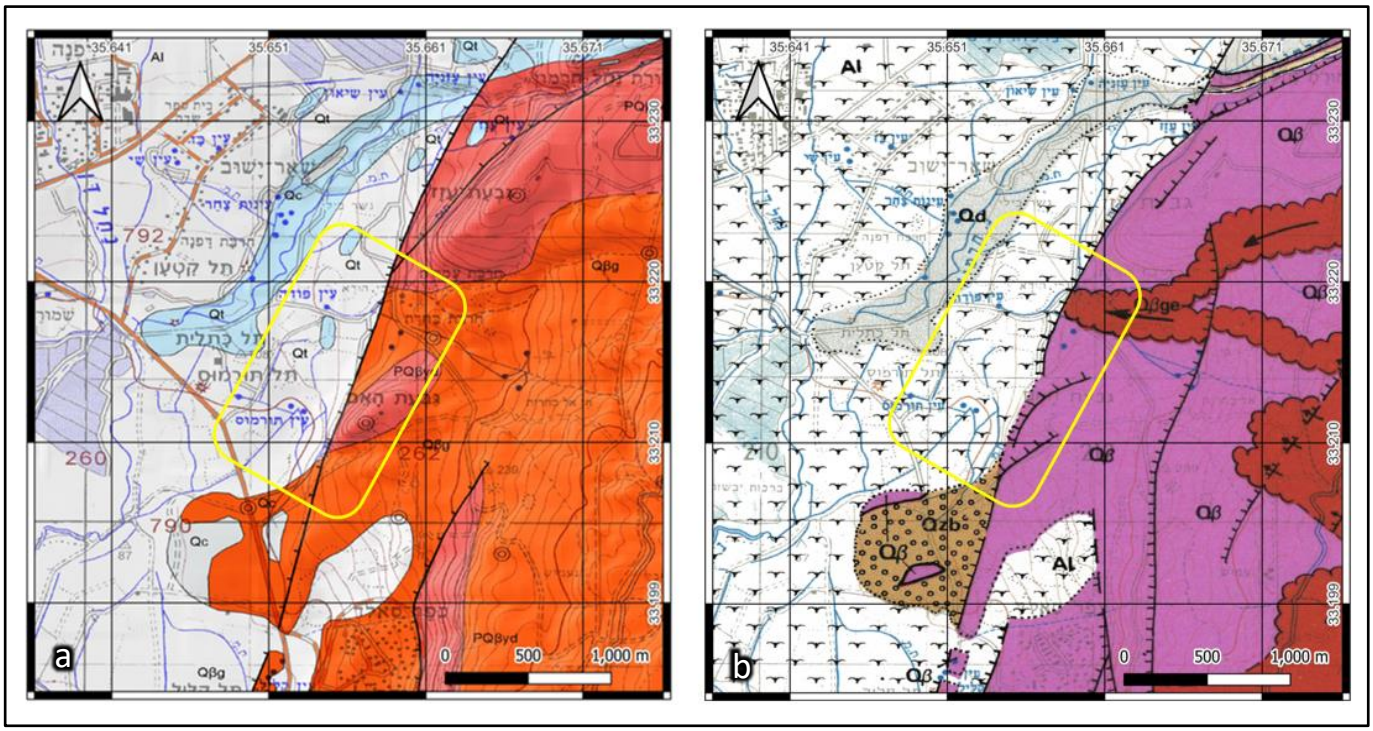

Figure 5 - (a) Nebi - Huda region above geological map after Sneh and Weinberger (2014), Red - Golan flows ($Q\beta g$), Orange -), Orange -Pleistocenic Yehudiyya – Dalwe Flows ($PQ\beta yd$) ; (b) Nebi - Huda region above geological map after Mor (1987), Red- Ein-Zivan flows ($Q\beta ge$), Purple – undivided basalt

Due to the extensive volcanic activity and difficulty in dating a large part of the Golan basalts, the division of the Bashan Group formations and their location in time and space is extremely challenging. Therefore, the geological maps of the area are generalized and show a few outcrops of flow fronts, contact lines, and divisions into detailed units (figure 5).

On the basis of Mor's (1993) division of the basalts according to their morphostratigraphy and radiometric ages (K-Ar dating), the volcanic rocks in the survey area can be subdivided into two mapping units (Mor, 1993; Weinstein et al., 2006). The flow marked red ($Q\beta ge$) (Fig.5b) is related to Ein-Zivan Basalt and the area marked purple ($Q\beta$) is related to general undivided Plio-Pleistocene basalts. On an updated map (Fig 5a) the Ein-Zivan flow is not mapped in detail and is marked ($Q\beta g$)

as the Golan flows, a generic name for Pleistocene basalt flows in the Golan Heights region.

The ‘Azaz Fault is an active left-lateral fault which detached a travertine unit, whose maximum deposition age is 25,300 ± 800 years (Heimann & Ron, 1987). According to geodetic measurements, the horizontal left- lateral movement rate is 1.2 -1.4 mm / year (Gomez, Karam, et al., 2007; Gomez, Nemer, et al., 2007; Nemer & Meghraoui, 2006; Reilinger et al., 2006; Sadeh et al., 2012). The average slip rate is 1.4-2 mm/year (Garfunkel, 1981; Gomez et al., 2003)

The aim of this research is to better understand the local lithological limits and structural features, especially the limits and extents of the basaltic flows in the Nebi-Huda region, their continuation in the basin under the sedimentary cover, as well as the underlying structural contacts which are not exposed. To do so, an innovative drone-based magnetic survey is used for the acquisition of high resolution aeromagnetic data (HRAM). Such a method allows mapping anomalies linked to subtle variations of magnetization (Nabighian et al., 2005), as are expected in the study, where the drone solution offers a suitable combination of spatial resolution and coverage speed as was presented in the Saint Kitts case study by Gavazzi et al. (2019).

1.3 Geomagnetic methods

1.3.1 Main principles

According to the geo-dynamo theory, electric currents and magnetic fields are created due to the rotation of the Earth, through a turbulent flow of the fluids that make up Earth’s outer core (Elsasser, 1956). This is an ongoing process known as the self-excited geo-dynamo. Globally, on average, the field intensity on Earth's surface ranges from 20,000 to 70,000 nT and varies according to position on the globe (mainly latitude).

The geomagnetic field measured above the surface is mainly composed of the effect of the dynamo field, but also of the effects of the magnetization of the different bodies within Earth's crust. The aim of magnetic surveys is to map the spatial variations (i.e. anomalies) in the magnetic field, which are created by these different bodies.

Magnetization of rocks can be described by intensity and direction. The magnetization can be of two natures: remanent and induced. Induced magnetization (for anisotropic material) is in the direction of the global ambient field. Remanent magnetization fixes the global field of the time of formation and is typical of volcanic rocks. In our case, we expect a superposition of induced and remanent magnetizations. The flows were not dramatically distorted or rotated strongly, and are still in the orientation of formation (Mor, 1986; Heimann & Ron, 1987). Thus we expect remanent magnetization to be collinear with the induced magnetization, i.e. in the direction of the current global field, or the opposite if formed in a period of geomagnetic reversal. In addition to the dynamo and crustal fields, measurements also include time-induced variations related to external sources (mainly due to solar winds). In this study such variations are considered as "noise" and are removed through data processing. As mentioned, a total magnetic field value measured at some point above the surface comprises a superposition of all sources from the earth's core up to solar winds. Therefore, the use of proper data processing tools is crucial for creating high-quality and interpretable magnetic maps.

Given the dominance of the geomagnetic component stemming from the geodynamo, the aim of any magnetic survey is to detect subtle spatial variations (anomalies) within a very large measured total magnetic field. To do so the magnetic anomaly field ($\vec{A}$) can be defined for each measuring point as

$$\vec{A} = \vec{B} - \vec{G},$$

(Eq 3)

where $\vec{B}$ is the total magnetic field, which is the measured field after removing all noises (including time induced variations), and $\vec{G}$ is the regional geomagnetic field due to the dynamo and other deep sources. For a large scale regional magnetic survey, $\vec{G}$ is commonly assumed to be given by the IGRF model (Alken et al., 2021), which is a mathematical model of the effect of the deep sources.

For technical reasons, only the intensity of the field (Total Magnetic Intensity or TMI) can be measured while in motion, and a TMI anomaly can be defined as

$$T = \left|\vec{B}\right| - \left|\vec{G}\right|, \qquad \textit{(Eq 4)}$$

and if we assume that the regional geomagnetic field is constant for the survey area and that the main TMI component is in the direction of the regional field, then

$$\mathrm{T} = \left|\vec{A}\right|, \qquad \textit{(Eq 5)}$$

where T is the value which will be transformed from the magnetometer output ($\vec{B}$ after filter corrections) and which will allow us to produce a local magnetic intensity map.

Lateral contact between units of different magnetization will generate anomalies; we expect to see lithological contacts due to structural features, conditions of formation, alteration and morphology both in the basement and sediment (Nabighian et al., 2005). Moreover, as the signal decreases quickly with distance, the survey strategy is to fly at a few different elevations to have different resolutions; high altitude for

targeting large primary elements, and low altitude with a higher data density for smaller targeted areas, with more subtle variations.

The impact of distance can easily be seen if we define sources as a cluster of small spherical dipole sources of radius *a*. The magnetic field $\vec{M}$ of such a source centered in *C* at observation point *P* is expressed by (Blakely, 1996)

(Eq 6)

$$\vec{M} = \frac{\mu_0}{4\pi}\frac{4\pi a^3}{3}\frac{j}{r^3}[3(\hat{j}\cdot\hat{r})\hat{r} - \hat{j}],$$

where μ_0 is the magnetic permeability of empty space, $\vec{J}$ is the vector and norm of the magnetization vector and r is defined as $\overrightarrow{PC} = \vec{r} = r \cdot \hat{r}$. In our case for each point all the values are assumed constant except the distance to the source r, therefore the magnetic field due the source decays as $\frac{1}{r^3}$ (Gavazzi et al., 2019).

1.3.2 High resolution aeromagnetic (HRAM) unmanned aerial vehicle (UAV) based survey

Owing to the extensive surface coverage possible and the wide range of resolvable targets, magnetic surveys have become a standard tool for geophysical and geological research, both for industrial and academic application (Calou & Munschy, 2020; Gavazzi et al., 2019; Nabighian et al., 2005). The choice between aerial and terrestrial- (or, more generally, surface) magnetic surveys is determined by the expected magnitude and size of the anomalies generated by the targets. The shape, size, and magnitude of an anomaly depends on the type of target (contrast in magnetic properties), its shape and the distance from it (le Maire et al., 2020).

Aerial surveys are more common, in which the measuring instrument is installed on an airplane, to map geological structures (e.g., Hinze et al., 2013) and to explore for

natural resources (e.g., Nabighian et al., 2005). The largest advantage of aerial surveys is that they allow investigation of deep sources when an extensive area is be mapped, and locate targets that produce strong, broad-scale magnetic anomalies which the magnetometer can detect remotely. Surveys from an airplane are usually limited to a minimum height of 100 m above the ground for safety reasons. Therefore, in many cases, the method is limited in terms of the resolution of the anomalies, and it is difficult to identify local lithological differences or local faults.

In ground surveys, a person or vehicle carries a magnetometer 10cm to 2m above the surface in order to locate shallow targets. Unexploded ordinance (UXO) (Munschy et al., 2007), buried pipes and other infrastructure (Gavazzi et al., 2019), shallow geology (Gavazzi et al., 2019), and archeology (Gavazzi et al., 2016, 2017; Fassbinder, 2017; Eppelbaum, 2021) are just some of the many applications in which targets can be detected using ground-borne magnetic surveys.

The main limitations of ground surveys are mobility and navigability (such as in areas where the topography or ground coverage makes it difficult to walk or drive).

In recent years, following technological advances reflected in the appearance of unmanned aerial vehicles (UAV) and the production of magnetometers which are smaller and lighter than in the past, the ability to make UAV-based aeromagnetic surveys has been demonstrated (Gavazzi et al., 2016, 2019). These surveys are intended to fill the gap between aerial and ground surveys by providing the ability to collect data at heights ranging from ground level to more than 200 m efficiently and continuously. Today, UAVs are mainly used for exploration surveys (Malehmir et al., 2017; Cunningham et al., 2018), but in recent years we have seen drone-based aeromagnetic surveys substitute for ground mapping (Cunningham, 2016; le Maire et al., 2020).

1.3.3 Previous research

Due to extensive volcanic activity the Golan Heights is a complex area for mapping, dating, and the use of application of geophysical methods. The area was initially mapped by Michelson and Mor (Mor, 1986; Mor et al., 1997) at a scale of 1:50,000, which defined the basaltic Bashan Group. Almost 20 years later Sneh and Weinberger (2003), mapped at the same scale, followed by more detailed mapping.

The basalts of the Bashan Group were formerly dated by Doron Mor and his team and Heimann and Ron (K/Ar) (Heimann, Ariel & Ron, 1993; Mor, 1993). The development of the 40Ar/39Ar dating method allowed precise age determinations (Behar et al., 2019; Feraud et al., 1983; Heimann et al., 1990; Inbar & Gilichinsky, 2009; Weinstein et al., 2006, 2013, 2020) .

Recently, eighteen age-dated samples from Pleistocene basalts expanded the dating of the Pleistocene-aged volcanics to between 1 million and 2.5 million years, completing the coverage of the Golan Heights (Behar et al., 2019). These measurements significantly contributed to establishing the ages of the Bashan Group basalts, showing a large variation in ages over a small geographical distance, so one must be careful of interpolation based on spot age measurements or surface geology.

Most paleomagnetism studies in the Golan Heights were published by Hagai Ron and his colleagues (Ron et al., 1984; Heimann & Ron, 1993; Hurwitz & Matmon, 2000; Behar et al., 2019; Frank et al., 2002, 2003; Taux et al, 2022). In 2019, a comprehensive study by Nicole Behar (Behar et al., 2019) measured and reanalyzed 40 samples collected by Hagai Ron, in addition to 51 samples collected by Behar and her associates.

'Azaz Fault in the center of the study area, was investigated by Ariel Heiman and Hagai Ron in their study of young faults bounding the Hula Valley (Heimann and Ron, 1987) and by Zilberman and his associates, who dug trenches to trace the Azaz fault (Zilberman et al., 2000). Schattner and Weinberger (2008) suggested, based on Rybakov et al.s' (1997) magnetic map, that since the mid-Pleistocene the Hula Basin entered a new geodynamic phase where the pull-apart mechanism was weakened due

to a NNW-striking cross-basin left-lateral fault. Politi (2011) presented comprehensive subsurface research that showed evidence for the branching of the Dead Sea Fault within the Hula basin.

Domzalski (1967) presented an aeromagnetic survey from 1km height over northern Israel including this study area. Schattner et al. (2019, 2022) mapped magnetic signatures in the Sea of Galilee region along roads surveys thousands of kilometers long with a portable magnetometer on a bicycle; Rybakov et al. (2011) investigated the source of the magnetic anomalies in the Levant Basin; Segev and Rybakov (2011) examined the magmatic history of the Western Galilee; Ten Brink et al (2007) surveyed from the air the magnetic anomalies of the Dead Sea. Ginzburg and Ben Avraham (1986) presented a map of magnetic anomalies integrating both lacustrine and land measurements in the Kinneret (Sea of Galilee) Basin. They showed strong anomalies on the eastern and northwestern slopes of the basin, indicating volcanic activity despite the basin's center being relatively magnetically quiet.

Ground magnetic surveys in the study area were conducted as part of introductory courses in geophysics at the Hebrew University, under the guidance of Amotz Agnon and Benjamin Medvedev. These findings showed the potential for finding magnetic anomalies and detecting the shifted location of the above-mentioned basalt flows.

2. Methods

This section describes methods pertinent mainly for drone based HRAM surveys.

2.1. Fluxgate magnetometer

Fluxgate magnetometers were first invented during World War II for detecting submarines. After the war, the primary use of the sensor evolved toward exploration. Due to their small size, ruggedness and low power consumption, fluxgate magnetometers are well suited for mounting on a drone for HRAM surveys (Calou & Munschy, 2020).

The cores of a fluxgate magnetometer consist of highly permeable material. The cores have primary and secondary windings around them. The primary windings are connected in opposite directions and saturated by current pulses twice per cycle. The secondary coils measure the difference in potential, that is relative to the intensity of the magnetic field along it (Telford et al., 1990). Usually, core and coil elements are placed orthogonally. This structure allows measurement of the three components of the magnetic field. These characteristics make the fluxgate magnetometer a relative instrument whose measurement resolution depends on a few variables like temperature and orientation. The calibration method of the sensor and the compensation of the effects of the drone on the measurement will be discussed later.

Even though Fluxgate magnetometers are vectorial sensors, due to a lack of sufficiently precise inertial measurement unit (IMU) systems, the components from aeromagnetic survey cannot be used directly for interpretation, and only the norm (intensity) of the total magnetic field can be used accurately (Calou and Munschy, 2020).

2.2. Survey design

The outline of the magnetic survey follows a protocol described by Reid (1980), which includes parallel (main) and perpendicular (tie) flight lines where the ratio of line spacing to height is 1:1, e.g., a flight at the height of 100 m will be spaced 100 m from one profile to its neighbor. In addition, we designed the survey so that the UAV will fly with a height to tie-line spacing ratio of at least 1:3, thus improving quality control and measurement noise reduction.

The survey comprises the following ten stages:

A. Fly at an altitude 100 m above the study area (Fig. 6) to map magnetic anomalies over a maximum area at a low resolution to assess the deeper and broader features.

B. Fly at 50 m above the study area to map magnetic anomalies over the whole area, obtaining higher-resolution data relative to the results at 100 m to assess shallower features.

C. Preliminary processing and interpretation of the data and calibrating the results according to the (Munschy *et al.*, 2007) method, using the Applimag software.

D. Selection of areas of interest for the low altitude flights.

E. Flying at an altitude of 25 m above areas of greater interest.

F. Extensive interpretation, transforming the data using potential theory tools, to get the best possible information on the sources (Munschy et al., 2007; Gavazzi et al., 2019).

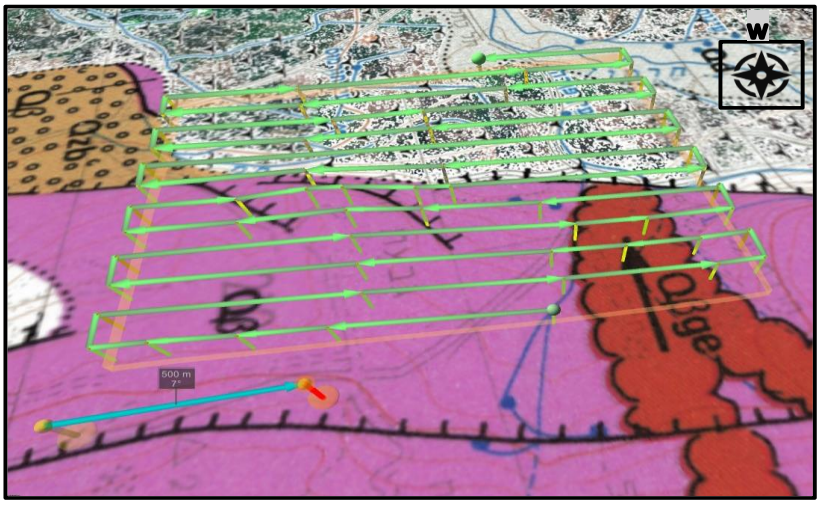

Figure 6 - 100m main-lines flight lines oblique view of Mor,1987

G. Comparing the results to previous magnetic mapping in the area (Kohn & Hassul, 2012; Paldor & Ziskind, 2013; Schechter & Bronstein, 2012), and to paleomagnetic measurements, collected and computed in the framework of an Introduction to Paleomagnetism course taught by HUJI's Prof Ron Shaar.

H. Explore the areas of interest that appear on the magnetic map using the drone-provided orthophoto.

I. Field excursion at the survey area.

In this survey we used a R3 FGM3D sensor from SENSYS GmbH mounted on a DJI Matrice 600 Pro drone (Fig. 7).

Figure 7 - Matrice 600 Pro with R3 double fluxgate magnetometer at base 5cm above the ground

2.3. Processing

2.3.1. Scalar calibration and magnetic compensation

This study uses a vector magnetometer. Since this is a relative magnetometer, affected by external variables such as temperature, it requires frequent calibration. To optimize the data quality that the device produces, we calibrate it at the beginning and end of each day of data collection. To calibrate, we need to correct three types of error, on each of the three components of the sensors (x,y,z); i.e., we must consider nine variables: three for the orthogonality of the measurement axes (u2, u3, u1), three for the shift (O1, O2, O3), and three for the sensitivities of the sensor (S1, S2, S3). Orthogonality is the difference between a perfect geometric orthogonality and the actual one, shift is the offset between actual and sensor zero value, and sensitivity is a matter of "gain" (difference between actual and registered variations). After performing a figure of merit (FOM), a procedure in which the sensor is flown at high altitude and the drone is rotating in any direction, the mathematical solution is obtained under two assumptions:

1. The intensity of the magnetic field is constant in the calibration area.
2. The difference between the measured and the actual magnetic field intensity is due solely to the magnetometer errors

Munschy et al. (2007) showed that the magnetic field vector (B) is given from the magnetometer output (F) by:

$$\begin{bmatrix} B_X \\ B_y \\ B_z \end{bmatrix} = \begin{bmatrix} 1 & 0 & 0 \\ -\sin(u_1) & \cos(u_1) & 0 \\ \sin(u_2) & \sin(u_3) & \sqrt{1-\sin^2(u_2)-\sin^2(u_3)} \end{bmatrix} \begin{bmatrix} S_1 & 0 & 0 \\ 0 & S_2 & 0 \\ 0 & 0 & S_3 \end{bmatrix} \begin{bmatrix} F_X \\ F_y \\ F_z \end{bmatrix} + \begin{bmatrix} O_1 \\ O_2 \\ O_3 \end{bmatrix}$$

Eq 7 – Equation for calculating a vector field from a calibrated magnetometer; B – Magnetic field Vector; F – Magnetometer output; u – lack of orthogonality; O– Offset; S- Sensitivity

Since the problem is not linear, we used the linearization and least-squares approach for linear regression presented by Olsen et al. (2003), in which we deduce the χ^2 for the measurement obtained by the sensor for each of the axes by:

$$\chi^2 = \sum \frac{\left|\vec{F}\right| - \left|\vec{B}\right|}{\sigma_B}$$

Eq 8 – Least-square test; F – Magnetometer output; B - Magnetic field intensity in the sensor calibration area in all directions; σ_B – Data error

Another issue with the magnetic measurement is the correction for the effects of the sensor carrier, called magnetic compensation. The magnetic effect of the UAV consists of a combination of four sources:

a. Remanent magnetization

b. Induced magnetization

c. Eddy currents

d. EM – Electromagnetic noises (telemetry and engines)

Munschy et al. (2007) showed that the calibration procedure also compensates for the remanent and induced magnetization of everything firmly attached to the sensor (i.e. the magnetometer shouldn't move relative to the carrier device to be compensated). We can calculate the amount of compensation required using the same scalar calibration equations (equations 1 and 2), where the remanent magnetization is parallel to the offset (O), and the induced magnetization is similar to both, the lack of orthogonality of the axes and the sensitivity of the sensor (S,u). The UAV is too slow to create a low frequency Eddy-current that will disturb the data measurement, and the EM noise is a high-frequency electrical noise filtered by the digitizer (Munschy et al., 2007).

After calibration, the standard-deviation (STD – "ect" in figures 8) of the data recorded during the calibration procedure decreases from more than 10nT to 1.4nT - 2.1 nT.

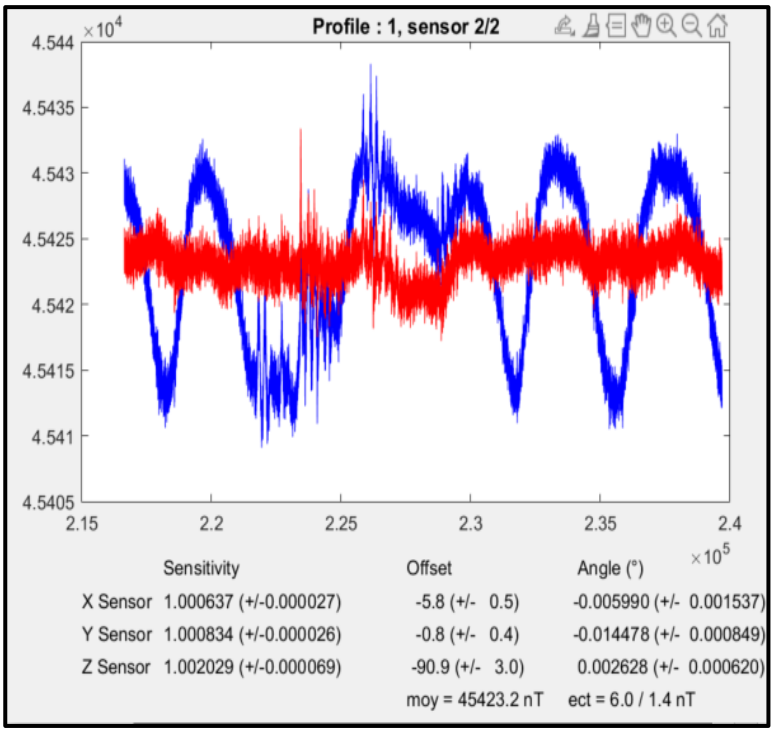

Figure 8 – Results of the recording during FOM, before correcting in blue and after correction in red. The computed corrected parameters are displayed at the bottom of the figure.

2.3.2. IGRF

The geomagnetic field is the main component of the measured total magnetic field (Campbell, 2003). The field is largely dipolar and Its amplitude at the research area is around $45x10^4nT$ according to the IGRF. The most commonly used model for the Earth's geomagnetic field and its secular variations is the International Geomagnetic Reference Field (IGRF) (Nabighian et al., 2005; Alken et al., 2021). In this study, due to the small survey area, the IGRF is less significant and changes by only a few nT (Fig.9) (Blakely, 1996). Indeed, IGRF is not meant to model precisely the regional magnetic field over such a small area, and so close to the various sources, and might be prone to errors of only a few nT. Thus, in the study, removal of the median value from the data is applied to correct for the regional field.

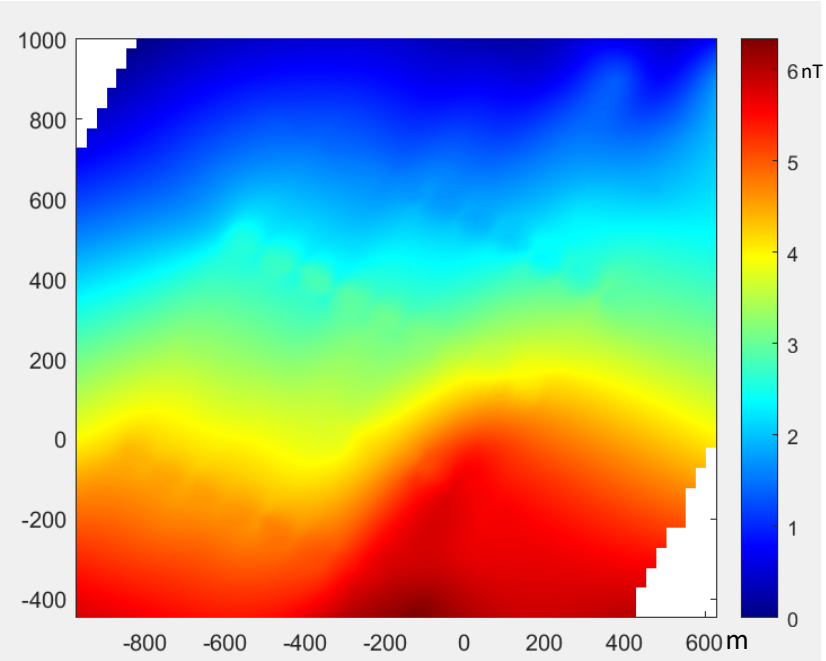

Figure 9 - -Differences between IGRF and median value at each point at the survey area by nT

2.3.3. Leveling

External field variations affect the magnetic data by adding a residual long-wavelength difference between adjacent flight lines. To correct the external field variations effect, also known as the leveling effect, the use of tie-lines perpendicular to the main lines is usually well suited. The tie-line spacing is larger than the spacing of the main-lines and has been chosen in the research to be three times the line spacing of the ‚main-lines (Nabighian et al., 2005).

The main principle of leveling is finding an offset correction for each line in order to minimize the differences at the crossing points between the main-lines and the tie-lines by the least-square fit (eq 8).

Because the survey lines are of relatively short duration, we can consider the time-induced variation to be constant along the profile, so a leveling correction that finds a constant value on each profile will correct the time-dependent variations.

2.3.4. Gridding

Because of the alignment of the magnetic measurements along the flight lines, and the high rate of measurements (200 Hz) for the R3 magnetometer, there is much more sampled data along the flight lines than across them (Fig.10),

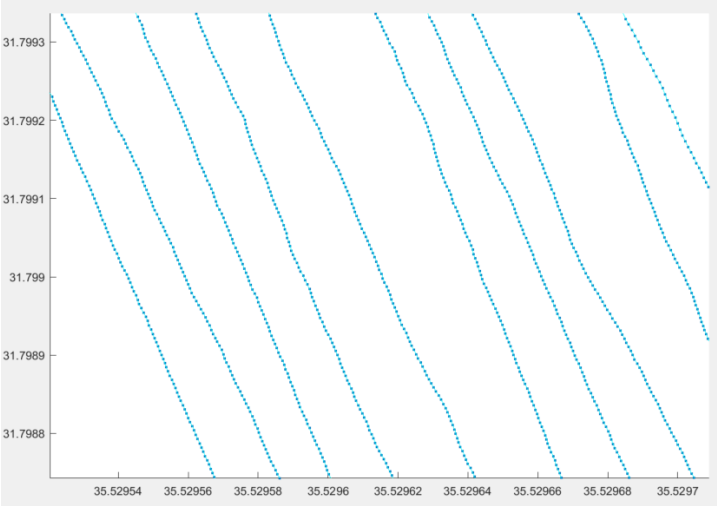

Figure 10 - Points of measurments along flight lines

To solve the issue of different density of point according to the direction of flight line, and get a same overall resolution, data is interpolated on a regular grid using the GRIDFIT modeling tool (Errico, 2006). GRIDFIT is a surface modeling tool which computes a regular 2D grid from scattered or regular data. After applying GRIDFIT the total magnetic intensity anomalies map is received.

2.4. Potential field transforms

2.4.1. Reduction to the pole (RTP)

Reduction to the pole (Baranov & Naudy, 1964) is a mathematical approach that transforms the measured magnetic data into the values it would have if it was measured with the magnetization and regional field both vertical. The method assumes that the

remanent magnetization is parallel to the geomagnetic field. Also, the method assumes that the regional field and the remanent fields of the objects are invariant over the survey area, which make that transformation not suitable for continent-scale studies (Nabighian *et al.*, 2005) but well-suited for this study. The method correct for the asymmetry of a magnetic anomaly as shown in Figure 11.

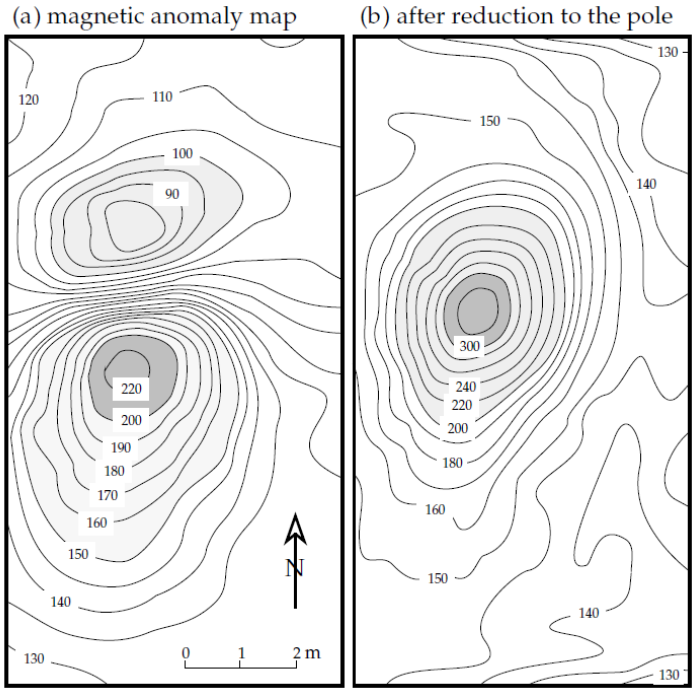

Figure 11 - Exemple of RTP contribution to the interpretation (after Linder et al. ,1984)

Gavazzi et al. (2019) showed that RTP transformation is well-suited to highlight limits and borders in a volcanic area because, if the flows are still in place, their remanent magnetization is in the direction of the regional field or opposite to it. Therefore, the position of sources is respectively given by positive or negative maxima.

2.4.2. Downward/Upward continuation

This is a method for approximating a map of magnetic anomalies at an altitude different than that at which it was measured. It is mainly used for approximating the distance from the magnetic source (Blakely, 1996). The basic principle is to increase the distance of the observed data to the distance at which the projected anomaly oscillates quickly; it will then be the maximum distance from the measured surface (Lowrie, 2007). It is worth mentioning that while upward continuation is a relatively stable procedure, downward continuation requires it to be combined with other methods (Blakely, 1996). This is mainly because the downward method demands all the anomalies to be at the same wavelength; if not the shorter one will start to oscillate first and the grid will saturate before going to a lower altitude. In addition, if the noise is of short wavelength, it will oscillate first (Pawlowski, 1995; Ravat, 2007; de Lépinay et al., 2021).

2.5. First order vertical derivative (FVD)

First order vertical derivative is one of the most common potential field methods. It corresponds to the vertical gradient of the measured data set (Blakely, 1996). The FVD transformation attenuates the long-wavelength anomalies and enhances the short-wavelengths. Therefore, vertical derivatives emphasize shallow and small anomalies while de-emphasizing deeper source bodies (Nabighian, 1984),. Also, the transform increases noise as it highlights the shorter wavelength signals.

2.6. Anisotropy of magnetic susceptibility (AMS)

The magnetic susceptibility is a unitless tensor $\mathrm{M} = \mathrm{XH}$ where M is the material's magnetism, X is the anisotropy tensor, and H is the magnetic field (Hrouda, 2007) . The eigenvectors of the anisotropy tensor define the magnetic fabric, where k_1 indicates the maximum eigenvalue in the anisotropy ellipsoid, which in elongated minerals is usually parallel to the longitudinal axis (Fig. 12). The method makes it possible to trace the flow directions of lava flows because, due to shearing forces, elongated minerals tend to line up with the flow direction (Tauxe, 2002).

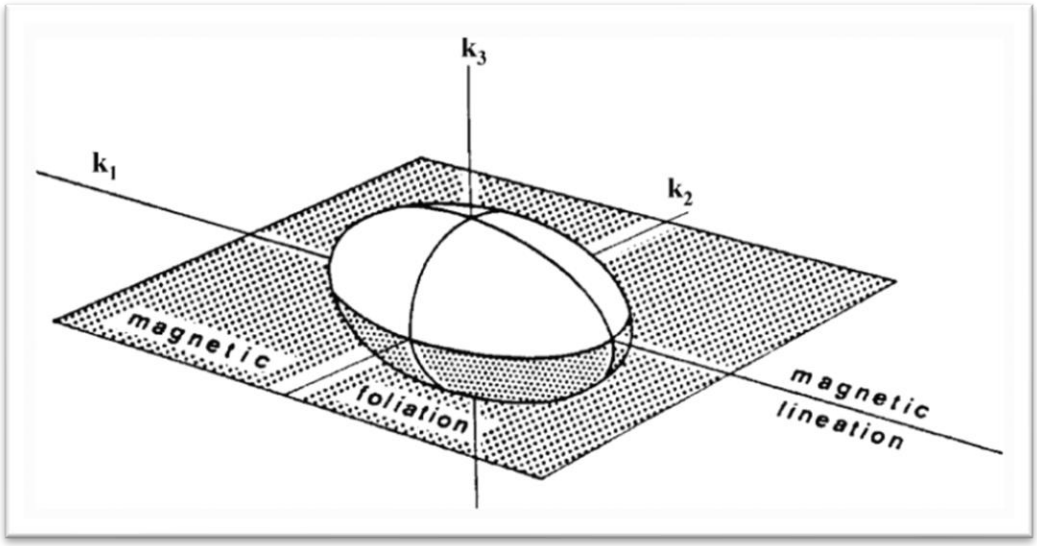

Figure 12 -Magnetic liniation and foliation on AMS elipsoide (Siegesmund et al.,1995)

The relevant indexes in characterizing the degree of anisotropy are lineation: $L = K_1/K_2$, foliation $F = K_2/K_3$, and the degree of anisotropy: $P = K_1/K_3$ (Hrouda, 2007).

3. Results

3.1. Magnetic maps

3.1.1. 100m

The drone was flown at one hundred meters height above ground level (AGL) and with 100m line spacing. The platform speed was always ten meters per second and the tie-line spacing was three hundred meters. The data seems to be clean with no visible heading errors or side effects.

We used RTP (Reduction to the Pole) to refine the anomaly boundaries. In addition, since there is a relatively sharp magnetic strength gradient between the survey area's east and its west, we used FVD to amplify the central area where shorter wavelength signals dominate.

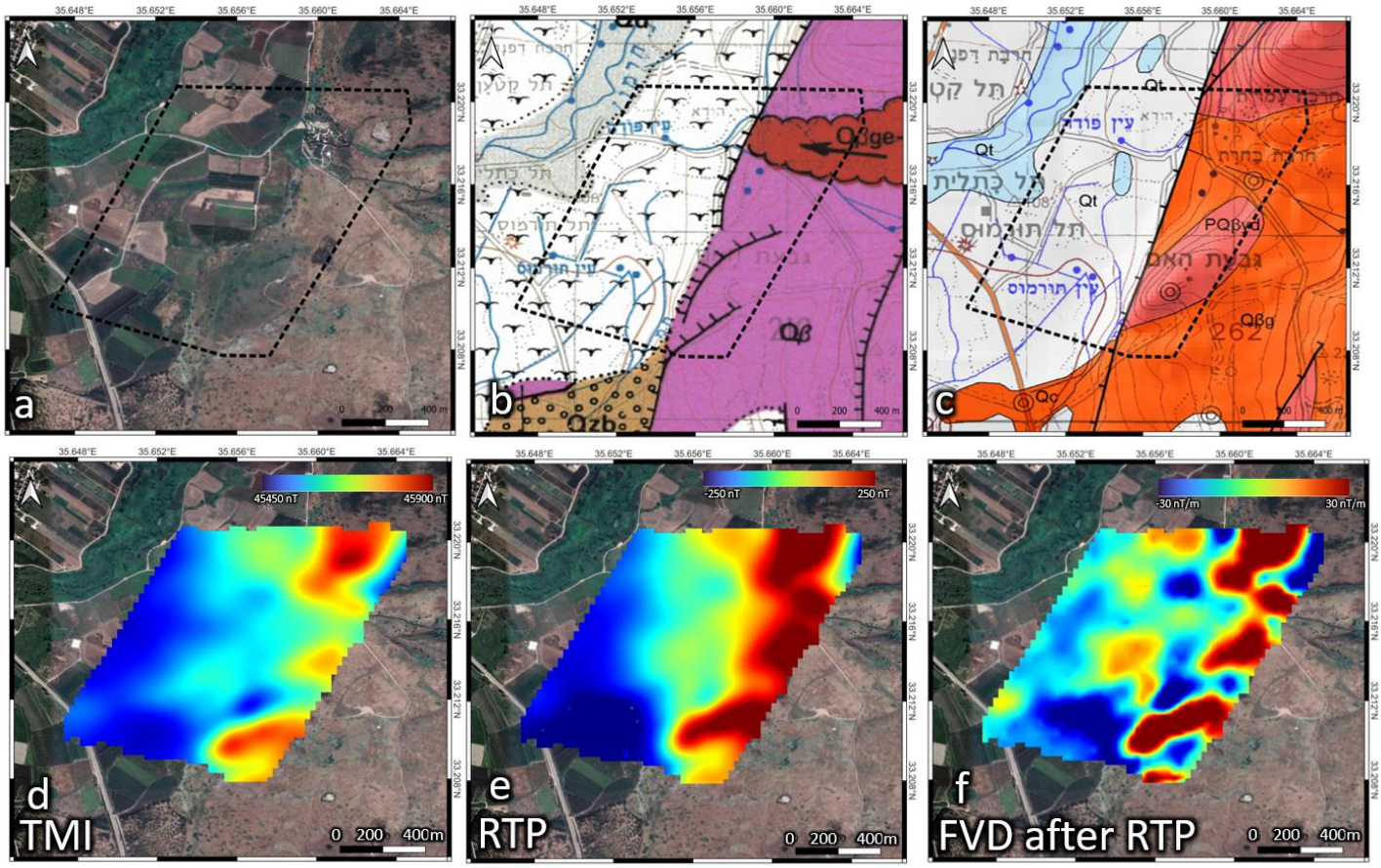

Figure 13 -The 100m and 50 m aeromagnetic survey borders: (a) above Google orthophoto, (b) above Mor's (1987) 1:50,000 geological map, (c) above Sneh&Weinberger (2014) 1:50,000 geological map ;Computed aeromagnetic maps at 100m altitude : (d) Total magnetic intensity anomalies (TMI), (e) Reduction to the pole (RTP), (f) First vertical derivative (FVD)

3.1.2. 50m

For higher data resolution, the sensor was flown at fifty meters AGL and covered the same area as the one hundred meters AGL survey at the same speed. Also, three magnetic maps were computed the same way as with the one hundred meters height (Fig. 14). On the FVD map small leveling effects can be seen along tie-lines but they do not disturb the interpretation. Correlation Is clearly vissible between the one hundred and the fifty meters AGL maps (Fig. 13-14).

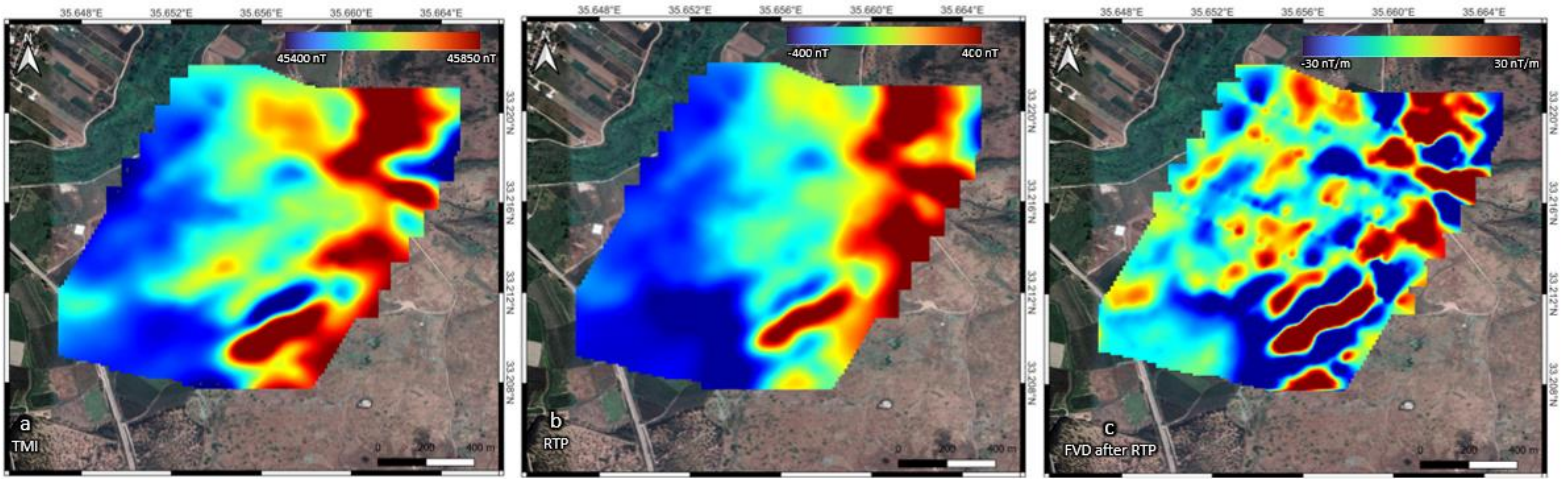

Figure 14 - Computed aeromagnetic maps at 50m altitude : (a) Total magnetic intensity anomalies (TMI), (b) Reduction to the pole (RTP), (c) First vertical derivative (FVD)

3.1.3. 25m

The lowest height at which the drone was allowed to fly is twenty-five meters AGL. The limitation is mainly due to anthropogenic infrastructure (powerlines, Nebi-Huda buildings, trees, etc.). The survey covered an area smaller than the fifty and the one hundred AGL surveys. The twenty-five meters AGL HRAM seems to enhance the midsize-wavelengths as we can see at the borders of the main basalt flows at Nebi-Huda.

The twenty-five meters AGL maps seem to show more detail than the previous maps at higher altitudes. They are not prone to noise except for a slight N-S leveling effect in the middle that appears mostly on the FVD, and does not disturb interpretation.

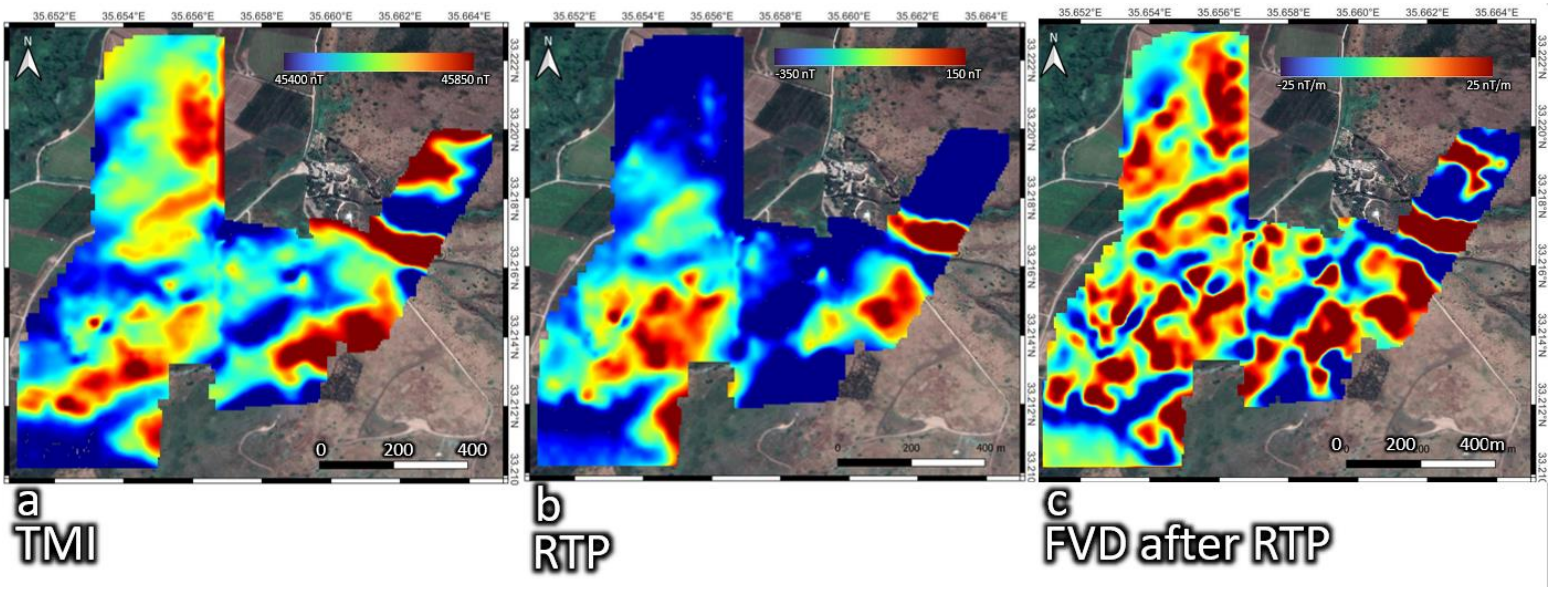

Figure 15 - Computed aeromagnetic maps at 25m altitude : (a) Total magnetic intensity anomalies (TMI), (b) Reduction to the pole (RTP), (c) First vertical derivative (FVD).

3.2. Orthophoto

An 2cm/pixel Orthophoto was made for better interpretation and for choosing the paleomagnetic sites. Figures 16 and 17 presents a case in which a high resolution orthophoto improves our ability to interpret a magnetic contact line, which appears to be the limit of the basalt flow.

Figure 16 - 2 cm/pixel Orthophoto of Nebi-Huda region with a 50m height magnetic TMI map .

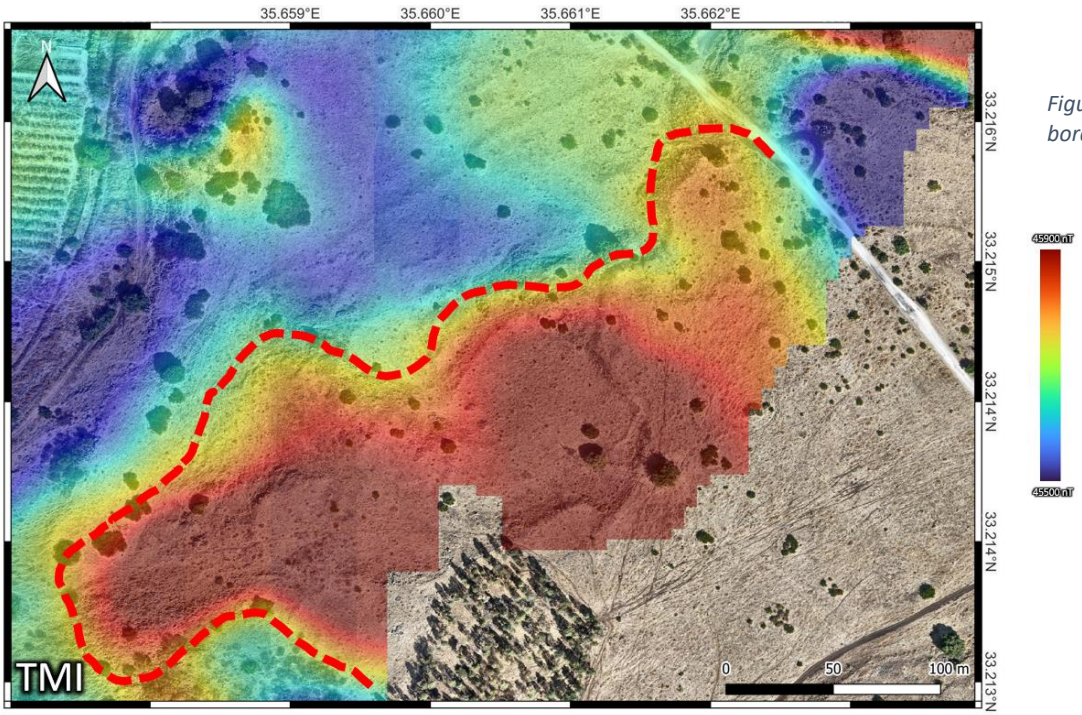

Figure 17– Corelation between visible flow borders and 50m height TMI map.

3.3. Paleomagnetic measurements

Twenty-six samples were measured from three different sites (Fig. 18, 19), in the framework of an "Introduction to Paleomagnetism" course given by Prof. Ron Shaar. The site names were designated as NBH (Nebi-Huda). Sites NBH01 and NBH03 were attributed to the same flow whereas site NBH02 to another flow further south. According to Sneh and Weinberger (2014), the two flows are associated with the Golan Formation. The samples were taken only from rocks exposed at the sites and allowed drilling and measurement by a sun compass. Each core is numbered in ascending order (Fig. 20). The cores were drilled using a fuel-driven cup drill with a diamond bit at the end, the rock being cooled using a continuous stream of water during drilling. The azimuth of the drilling was measured using a sundial and Brunton compass. A standard length of 2.2 cm used for the cores samples.

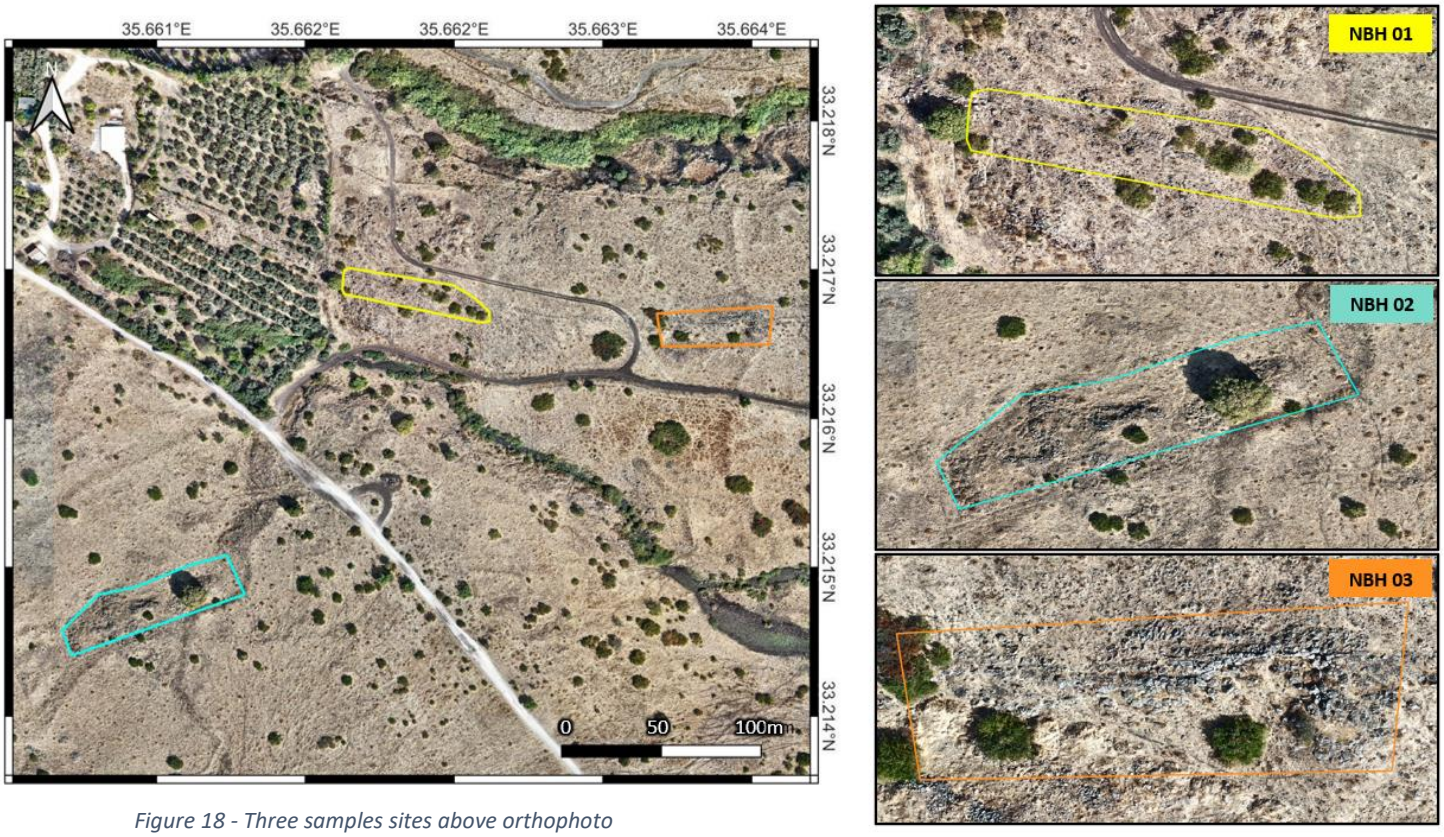

Figure 18 - Three samples sites above orthophoto

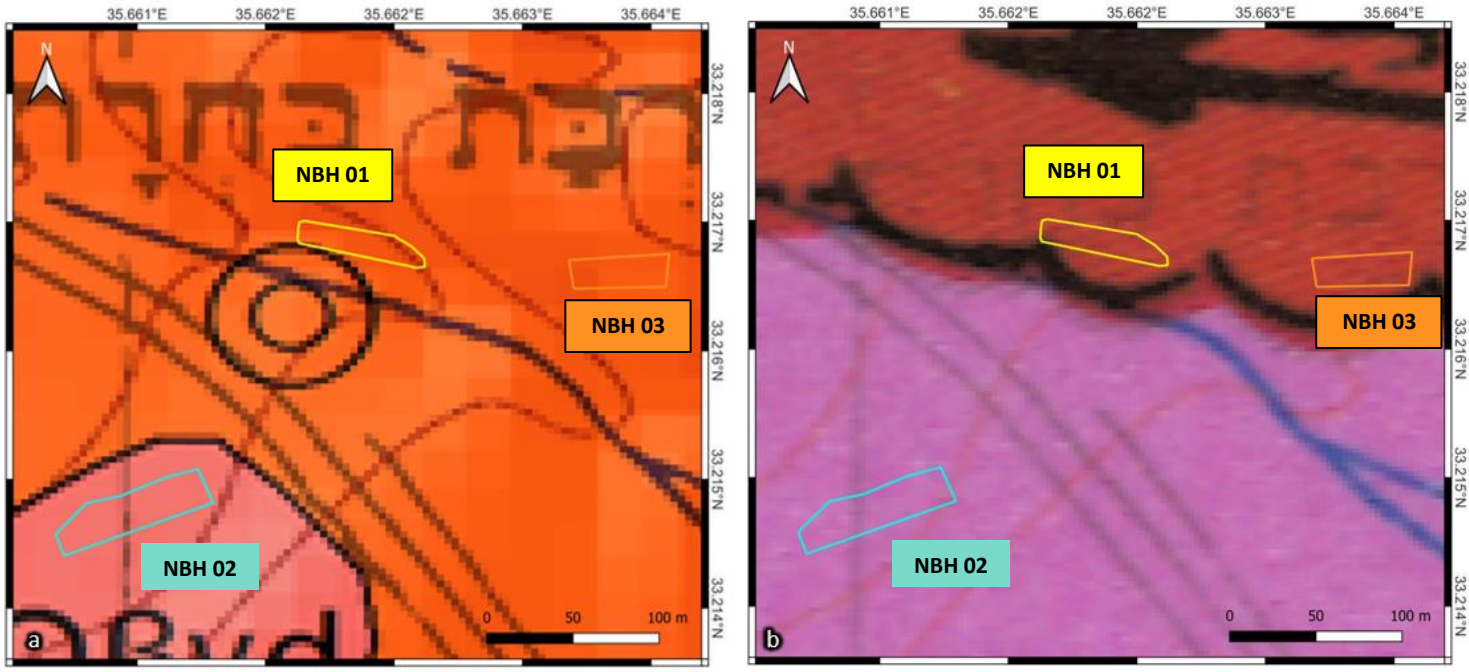

Figure 19 - The three paleomagnetic sites above: (a) Sneh and Weinberger (2014) geological map, (b) Mor (1987) geological map

Figure 20 - Cores positioning at NBH01 site

Although the results of the alternating-field (AF) and the Thermal measurements (see section 7 appendix) where not useful for determining precise and accurate paleomagnetic direction, we can conclude that all the eruptions erupted when the Earth's magnetic field was in a normal direction. From the AMS thermomagnetic graphs and the hysteresis, we deduced that NBH 02 (Fig.21) comprises a combination of pyrrhotite (200°C) and titanomagnetite or magnetite with some percentage of residual metals (e.g. Al or Mg) (400°C). Hence, NBH02 samples a different flow from the one sampled NBH01 and NBH03 (Fig.21).

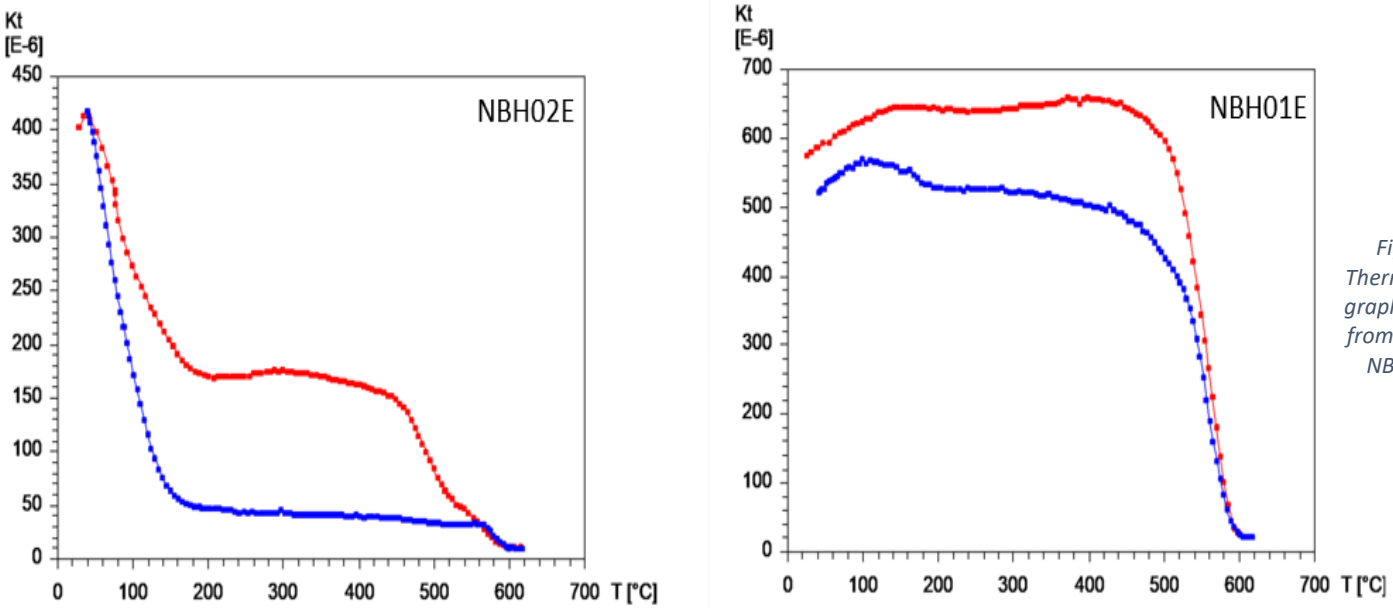

Figure 21 - Thermomagnetic graph of samples from NBH01 and NBH02 sites.

From the AMS measurements we infer that NBH 01 and NBH 02 have the same K1 direction indicating that they might have erupted over a similar topographic gradient (Fig. 22 and Appendix).

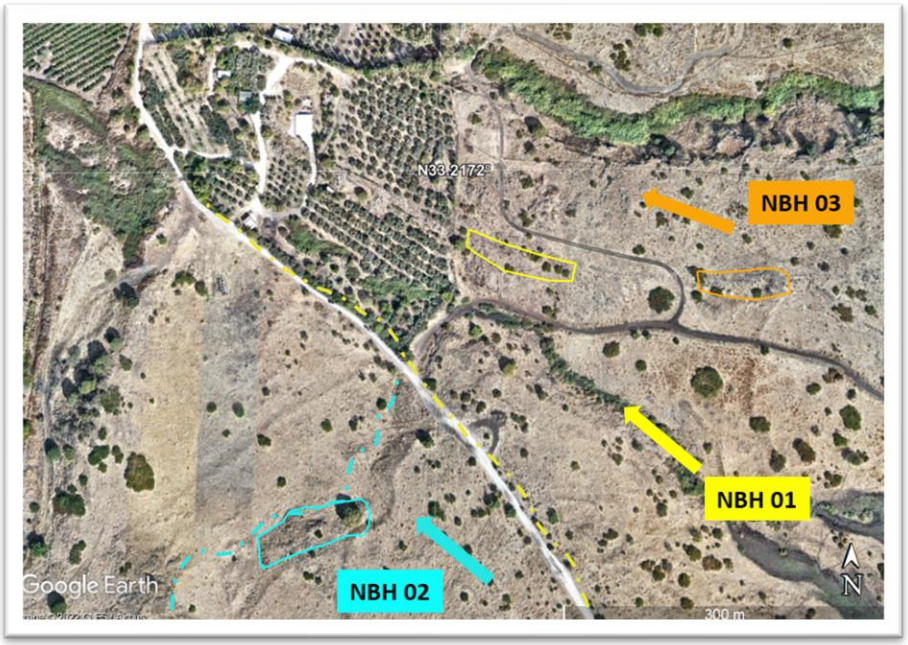

Figure 22 - Interpetation of the AMS results, orthophoto and fields; Dashed yellow and blue lines represent the contacts between the flows.

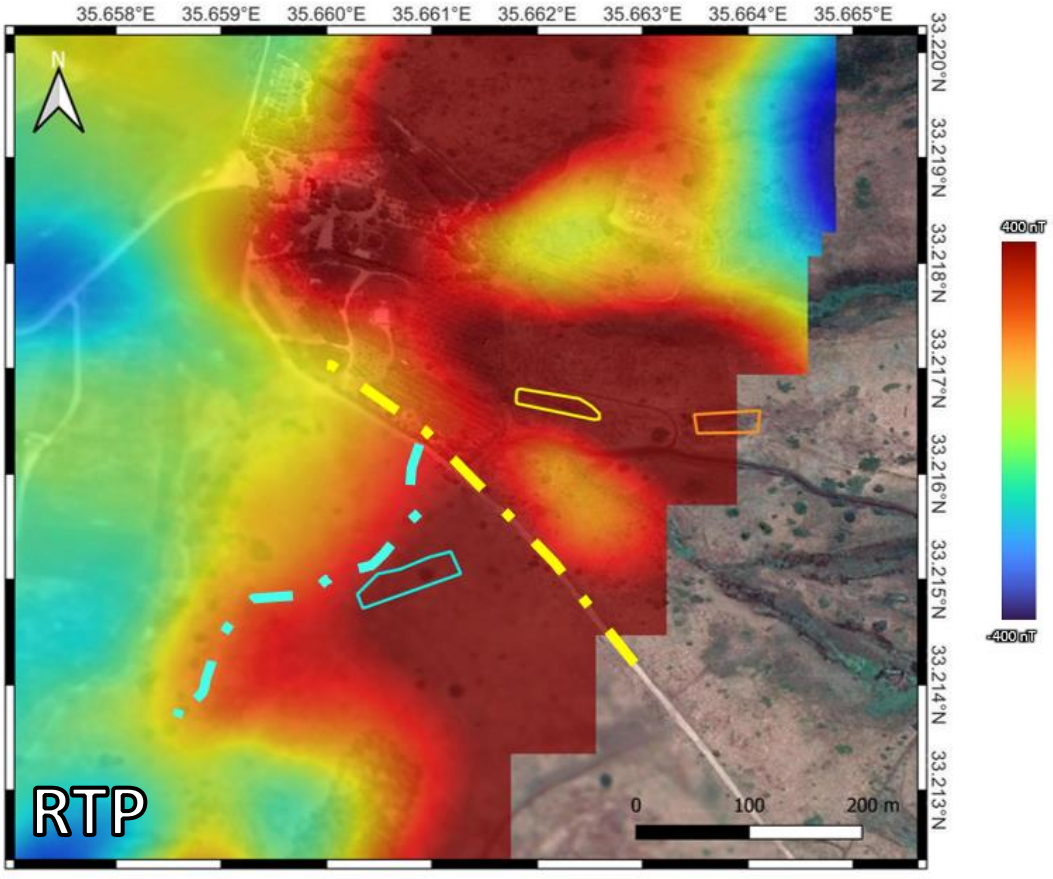

Figure 23 - Paleomagnetic results above RTP aeromagnetic map from 50m AGL survey height

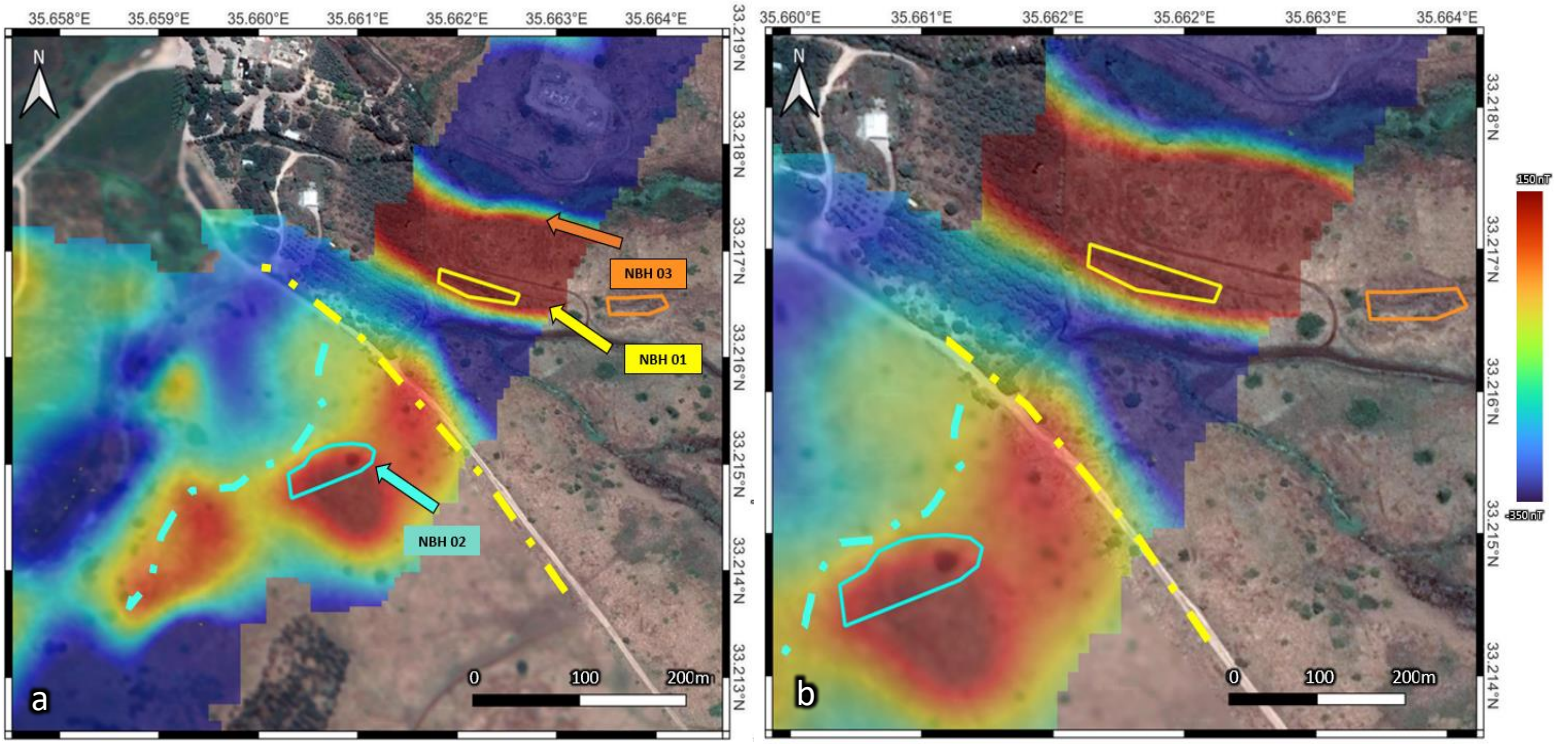

Figure 24 - Paleomagnetic sites and flows AMS directions; (a) above RTP aeromagnetic map from 25m height, (b) Zoomed in on a

The lateral differentiation between the flows is demonstrated in figures 23 and 24. At twenty-five meters altitude the limits of the NBH01,3 flow are better defined than at fifty meters.

4. Discussion

4.1. First order interpretation

4.1.1. Main features

Magnetic maps collected at one-hundred meters AGL (Fig. 13) were used for a first order interpretation. The aim of such first order interpretation is to identify the deep sources which produce large wavelength anomalies. Large wavelengths can be due to either deep and vertical contact, or shallower non-vertical contacts. Most of the

interpretation is made on the RTP maps, while other maps are mainly used to evaluate the interpretation.

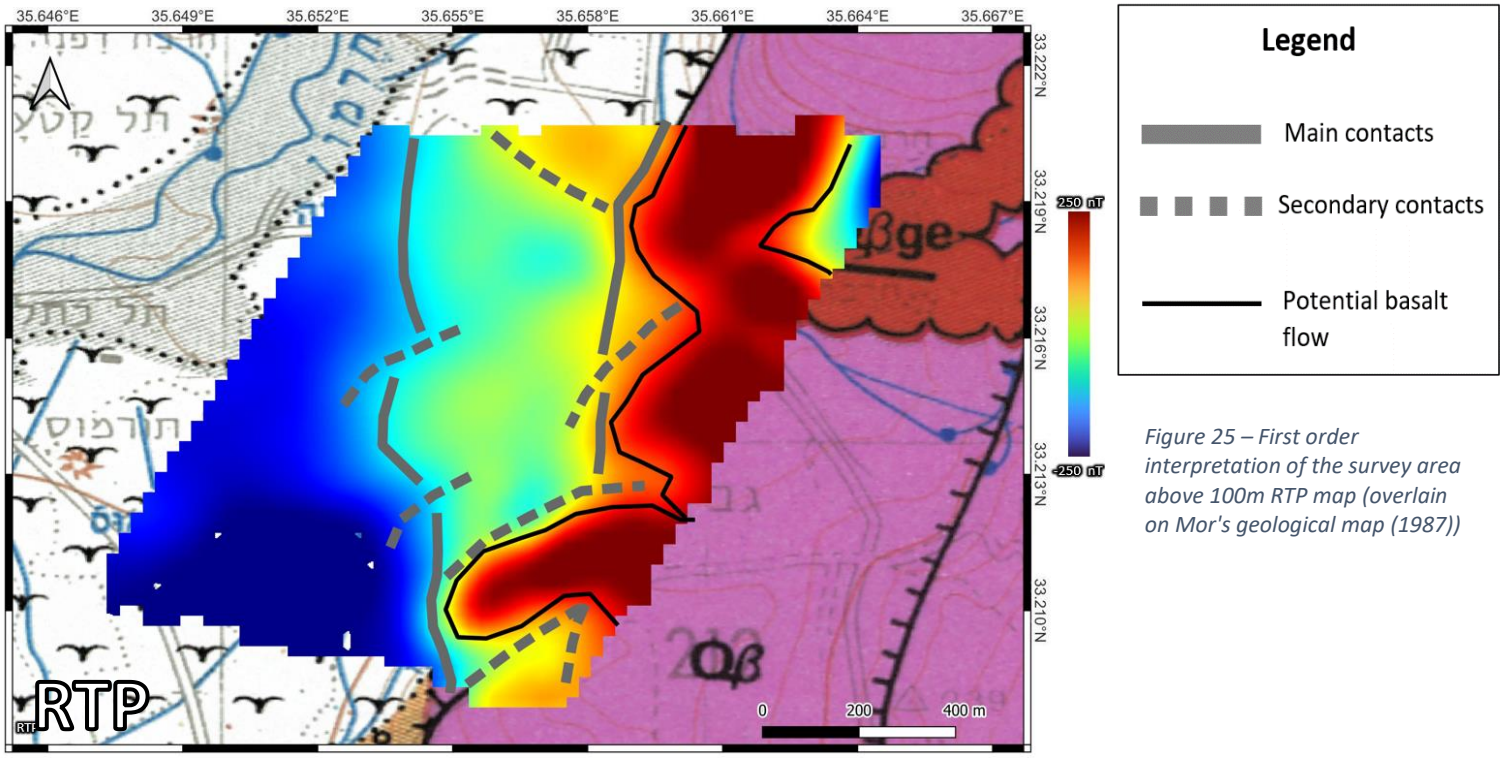

Figure 25 – First order interpretation of the survey area above 100m RTP map (overlain on Mor's geological map (1987))

The RTP anomaly map of 100m AGL (Fig. 25) shows a clear distinction between the basaltic Golan Heights slopes (positive residual) and the sediment covered Hula Basin (negative residual). The Golan Formation flows are all in the normal magnetic direction and have relatively distinctive first order borders.

Two possible faults with a north-south strike are identified and presented on the map as the Main contact lines. The eastern one also appears on the surface and on the geological maps and is marked as the main component of the 'Azaz Fault (Fig. 5, 13 (b,c), 25) (Politi, 2011; Politi & Agnon, 2009), while the western one was not exposed and was previously unknown. The main component of the movement along the marginal faults of the eastern part of the Hula Basin are on dip-slip faults with dominant vertical movement (Freund, 1970; Mor & Steinitz, 1983). The faults are compatible with the record of stress analysis by Eyal (1996) based on Heimann and Ron's work (1987). Politi (2011) characterized the of 'Azaz Fault as a marginal fault

with a main dip-slip component with respect to the Sion Fault, which was controlled mainly by a strike-slip regime. It is part of the shear zone fault system, which changes its faulting characteristics over a short distance (Politi, 2011). A suitable analogy for the structure we identified here is the fault escarpment west of the Dead Sea (Agnon, 1983). The structure of the fault scarp seems to fit the hierarchic three-dimensional character and slip-partitioning in the western Dead Sea pull-apart that Agnon (1983) and later Sagy et al. (2003) proposed (Fig. 26).

The dotted lines in Fig. 25 seem to represent the echelon-stepped faults proposed by Heiman and Ron (1987), and later presented in detail by Heimann et al (2009), which uplifted Givat-HaEm and the other hills at the area.

Between the two faults, at the transition zone (values around zero at Fig. 25), some weak anomalies appear at the resolution of the current flight altitude. And therefore a more detailed interpretation from higher resolution data is needed.

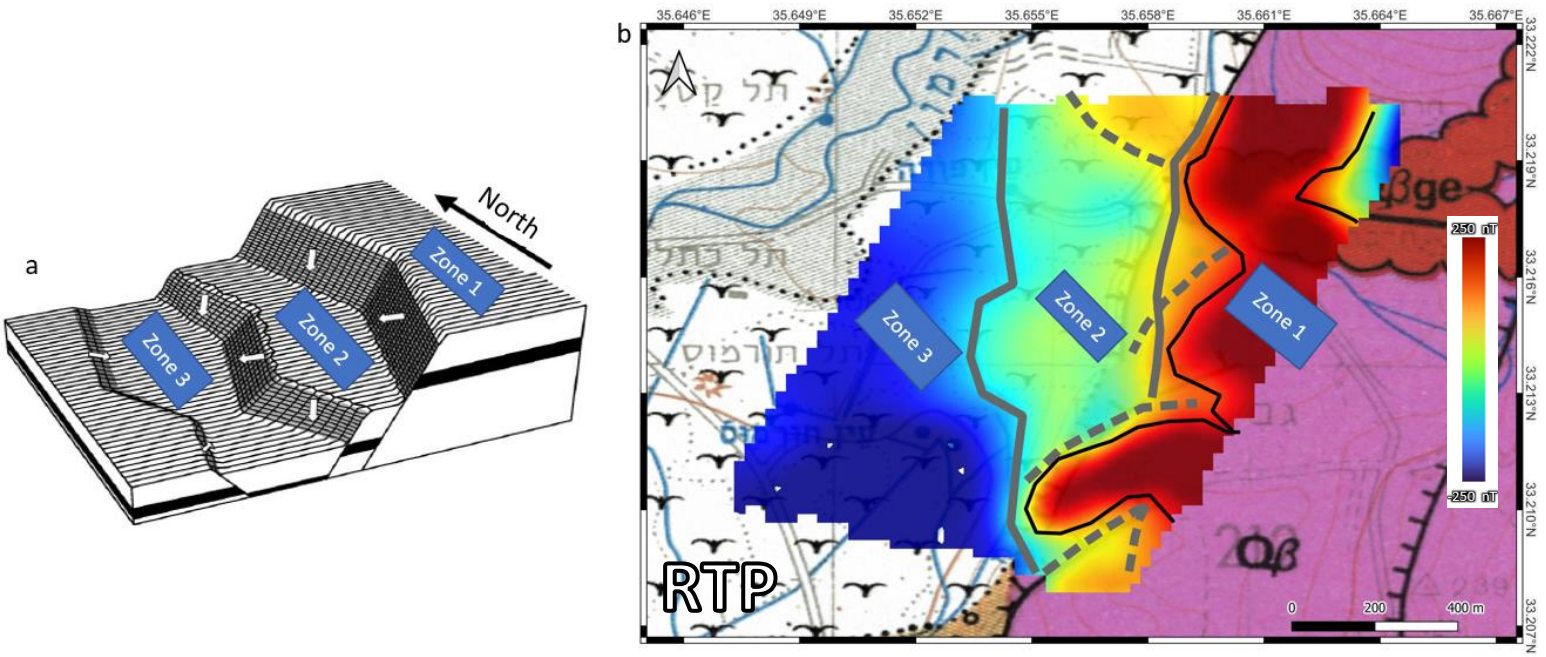

Figure 26 - Corellation between (a) schematic idealized configuration of the four dominant fault sets along the western margin of the Dead Sea (after Sagy et al.,2003), (b) Interpretation of the main features following 100m RTP magnetic map (above Mor,1987), Zone 1 – Golan Slopes, Zone 2 – transition zone, Zone 3 – Hula Basin sediments.

4.1.2 Normal magnetic direction of Givat-HaEm

According to Heimann (1990) the K/Ar age of the Givat-HaEm basalts is 1.22Ma. The Cobb -Mountain event is a short normal polarity event within the long Matuyama Chron (Mankinen et al., 1978). In the RTP magnetic map (Fig.26) all the main basalt flows (black lines) correlate to strong positive values, which means they have a normal direction of magnetization. Hence the Yehudiyya-Dalwe flows, which are attributed to Givat-HaEm fit recent models of the Cobb Mountain event occurring between 1.178Ma and 1.215Ma (Channell, 2017). Another possibility is that the Givat-HaEm flow is younger than the measured K/Ar age and is part of the late Pleistocene Golan Flows.

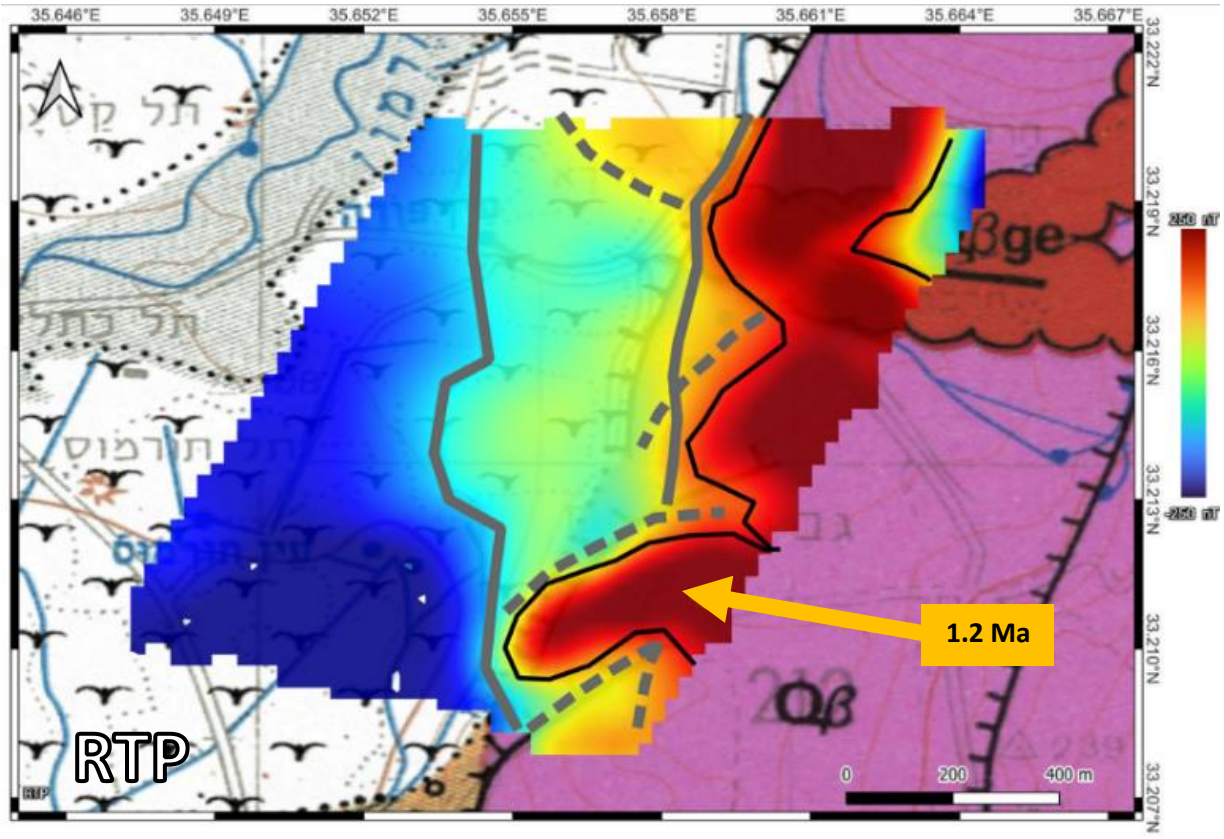

Figure 27 – Givat-HaEm location and its K/Ar age according to Heimann (1990) above the maps from figure 25.

4.2 Higher resolution interpretation

4.2.1 Second order faults

The 50 m survey allows us to assess features subtler than the 100 m survey. Three main groups of second-order faults can be interpreted in the area (Fig 28). The first, marked orange in Fig 28, is the one with the most widespread distribution in the region. Faults in this group strike 030°/210° ±10° and fit the direction of the two main faults at the area. The second group is marked in pink. Its orientation is 060°/240° ±10° and it correlates to the echelon feature detected in the 100m height maps (Fig. 26 dotted lines). The last group is marked in blue and strikes 320°/140° which correlate with the regional cross-nature of the slip-partitioned faulting of the eastern margins of the Hula Basin (Heimann & Ron, 1987; Politi, 2011; Politi & Agnon, 2009) and the western Dead Sea pull apart (Sagy et al., 2003).

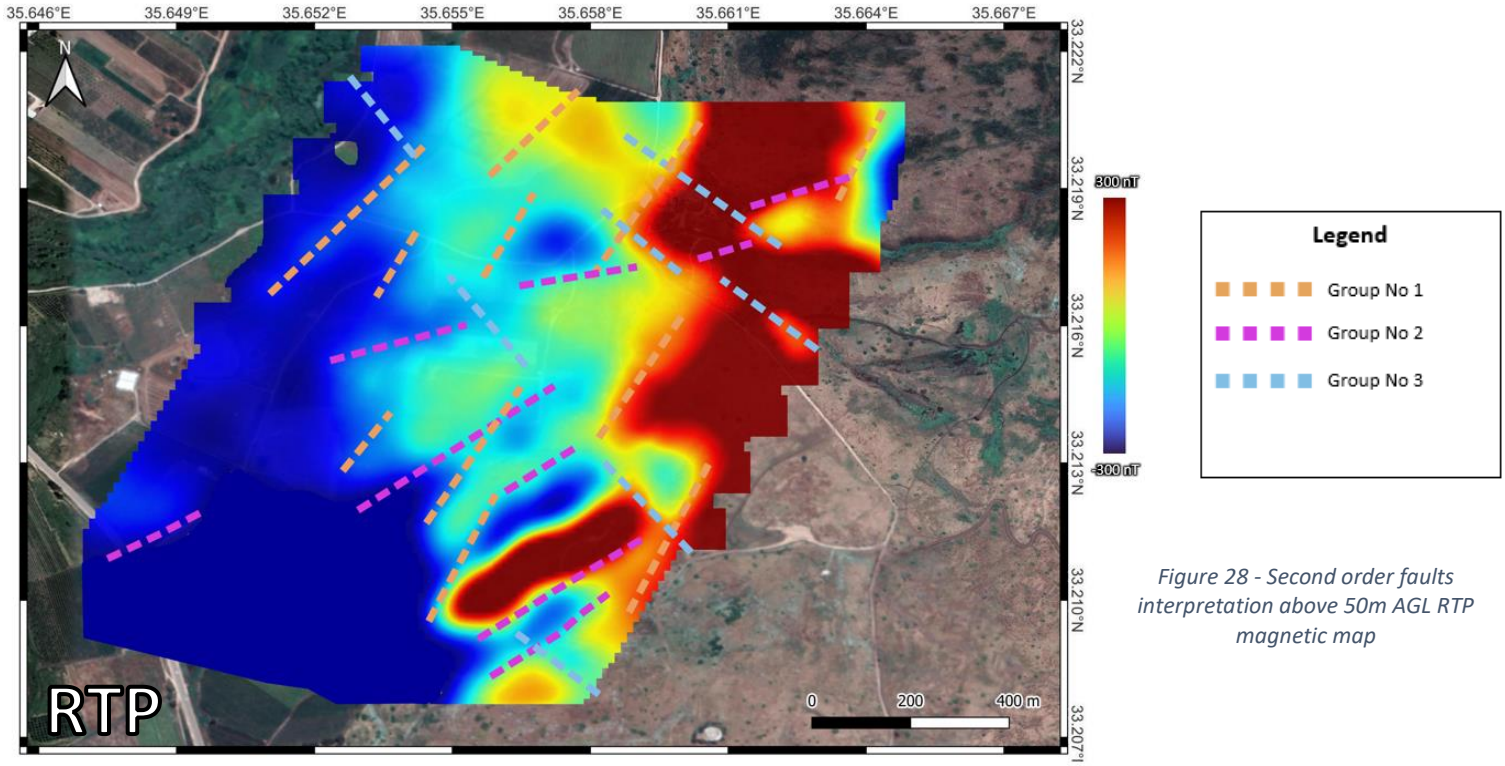

Figure 28 - Second order faults interpretation above 50m AGL RTP magnetic map

4.2.2 The Golan Flows

The fifty and twenty-five meter AGL magnetic maps allow more precise interpretation of the Golan Flows in zones 1 and 2 (Fig. 26). Taking into account the geological maps, paleomagnetic measurements, orthophoto and this research's aeromagnetic map, the Golan Flows in the survey region can be divided into five different flows (Fig. 29-30).

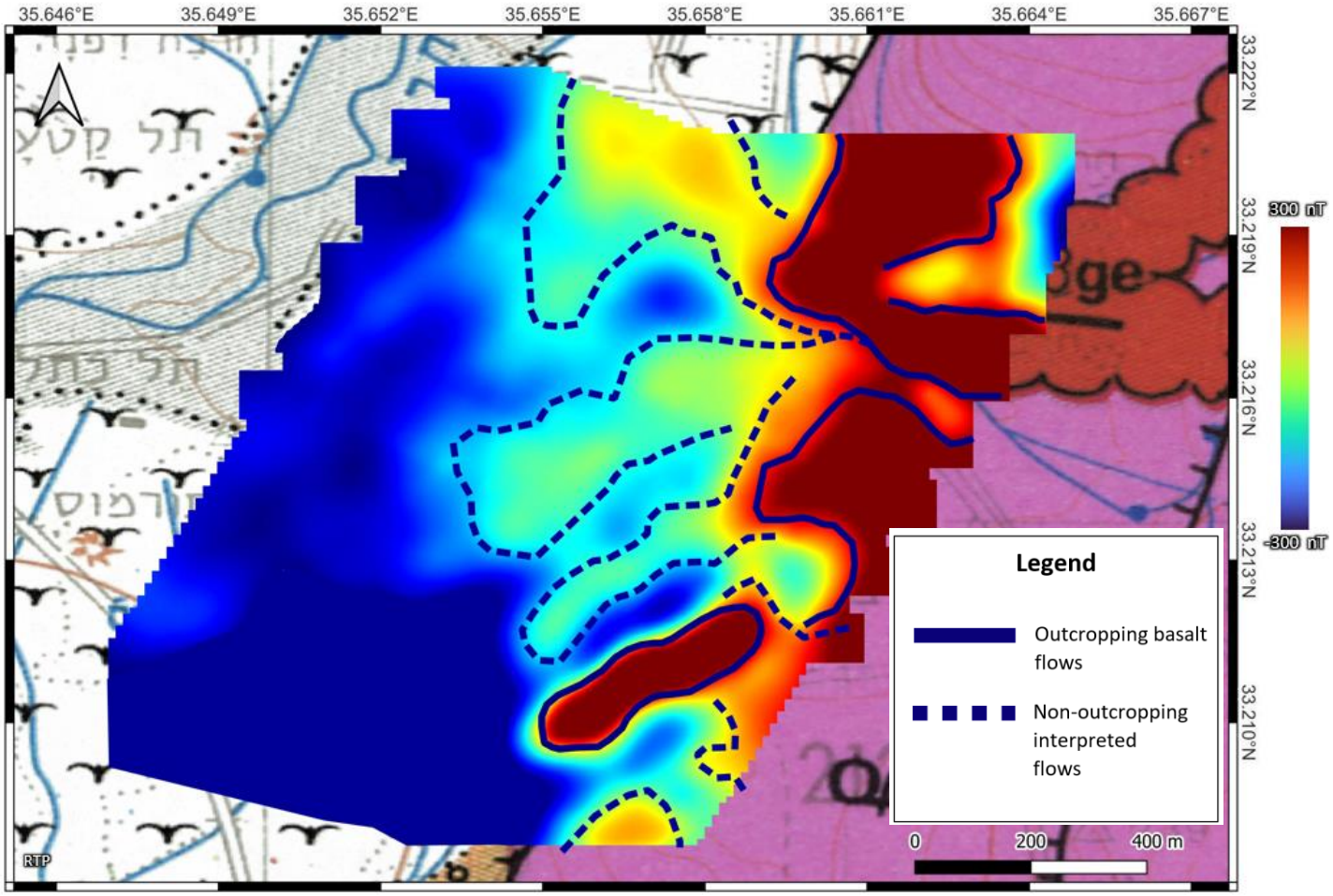

Figure 29 - Lithological interpretation of the survey area above 50m RTP map (Above Mor's geological map (1987))

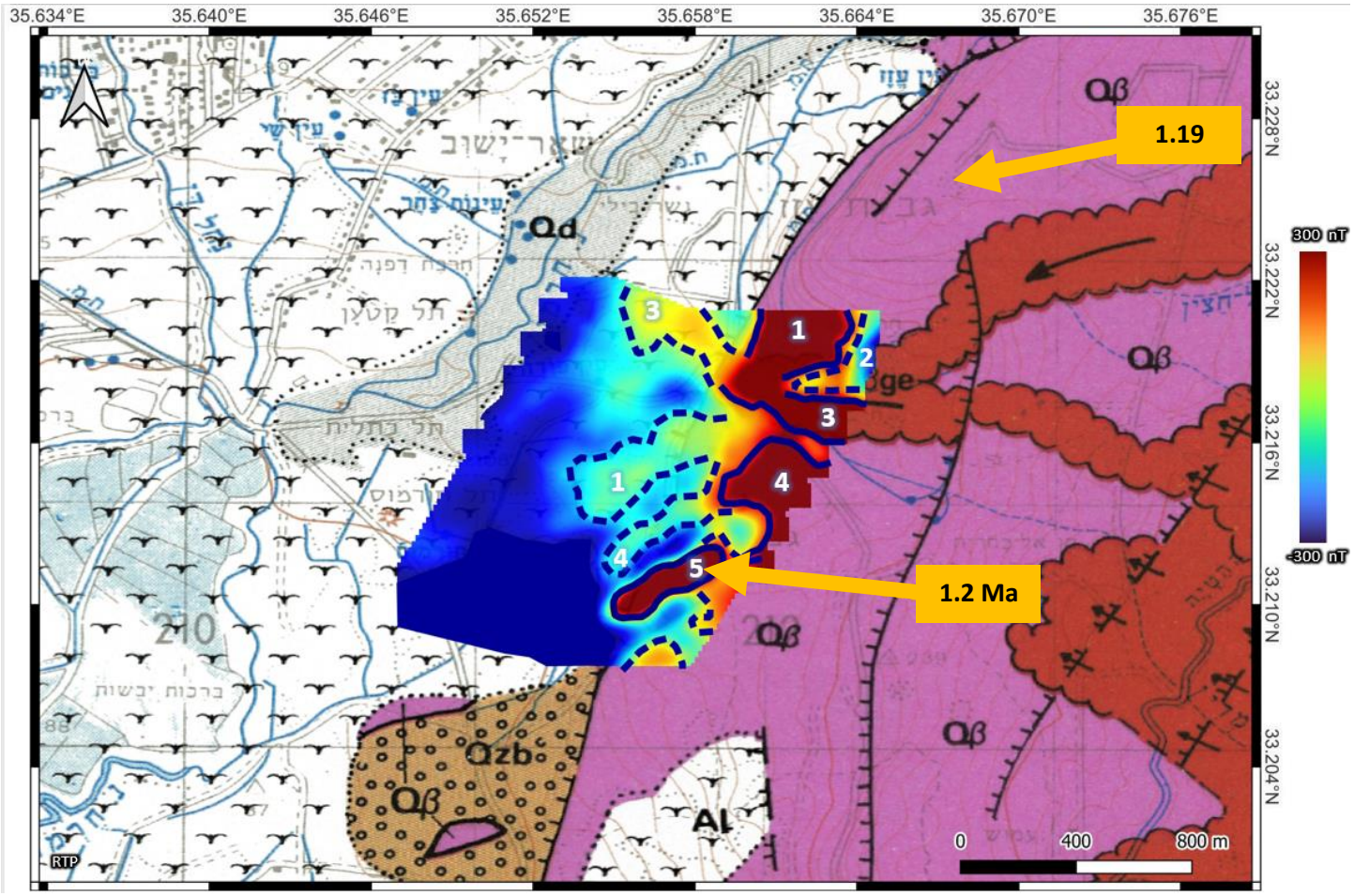

Figure 30 - Flows interpretation above 50m RTP map (above Mor's geological map (1987)) ; Arrows present the places where Heimann (1990) sampled K/Ar ages (orange numbers); the numbers of the flows east and west to 'Azaz Fault are marked in white.

The northernmost (marked as F1 in figure 30) has a high magnetic intensity with normal magnetic direction. It is elongated along 240°/60° and located on the slopes of 'Azaz Hill. According to Sneh and Weinberger (2014), it is related to the youngest basalts of the Yehudiyya-Dalwe flows (Fig.5, Appendix). Still, it is more likely attributed to the late Pleistocene Ein-Zivan Flows, which streamed over the Yehudiyya-Dalwe flows and comprise the 'Azaz Hill. This hypothesis is based on a possible adjacent continuation of that flow that appears on the western side of the 'Azaz Fault. The anomaly is of lower amplitude at fifty meters AGL (~50nT) and higher at twenty-five meters AGL (Fig. 31,32). The contour is dashed as a possible continuation of the fault, due to its similar orientation and proportions, after some lateral detachment by the 'Azaz Fault. Also, the flow seems to have an internal fractioning structure due to

faulting (Fig. 31,32). This is a similar phenomenon to those presented in some other recent aeromagnetic researches (Gavazzi et al., 2019; le Maire et al., 2020).

Flow F2 had acquired reverse polarity, with flow trending from east to west. The flow seems to correlate to the V shape within the Ein Zivan Flow in the eastern part of Mor's map (Fig. 29-30). Flow F2 can be attributed to some Pleistocene Yehudiyya-Dalwe flows from the reversed geomagnetic period postdating the ~Cobb Mountain polarity event.

Flow F3 features a normal polarity. Its western part is laterally well-defined and is attributed to the Ein Zivan Flow (NBH 01 and 03 from Fig. 22,23). The western part of flow F3 displays a lower amplitude on the 25m AGL maps than that of the other flows (Fig. 31,32). There could be several reasons for this, or a combination thereof. The first is that the flow is deeper than the others. Second, the flow has a lower magnetic susceptibility relative to the others. The third is a strong remanent component whose direction is far from that of the regional field. The fourth is a sediment cover of mainly diamagnetic character. Fifth is an erosion of ferromagnetic minerals. Also, the western part of the flow appears to be fractured due to detachment.

The fourth flow may have resulted over a few different periods due to its visible front flows (Fig. 16,17), and their the two magnetic directions were combined within the paleomagnetic measurements (Fig. 22-24). The continuation of the flow in Zone 2 is mostly underground. The shape of the contiguous anomaly suggests that the flow did not experience a significant detachment.

Flow F5 may correspond to a subsection of the Yehudiyya-Dalwe flows, as detailed in section 4.1.2. In the 100m and 50m AGL maps (Fig. 25-29) it appears as though the flow is crossing the main 'Azaz fault, and around it there are some crossing push-up faults, as Heimann and Ron and later Zilberman et al. have detailed (Mor, 1986; Zilberman et al., 2000).

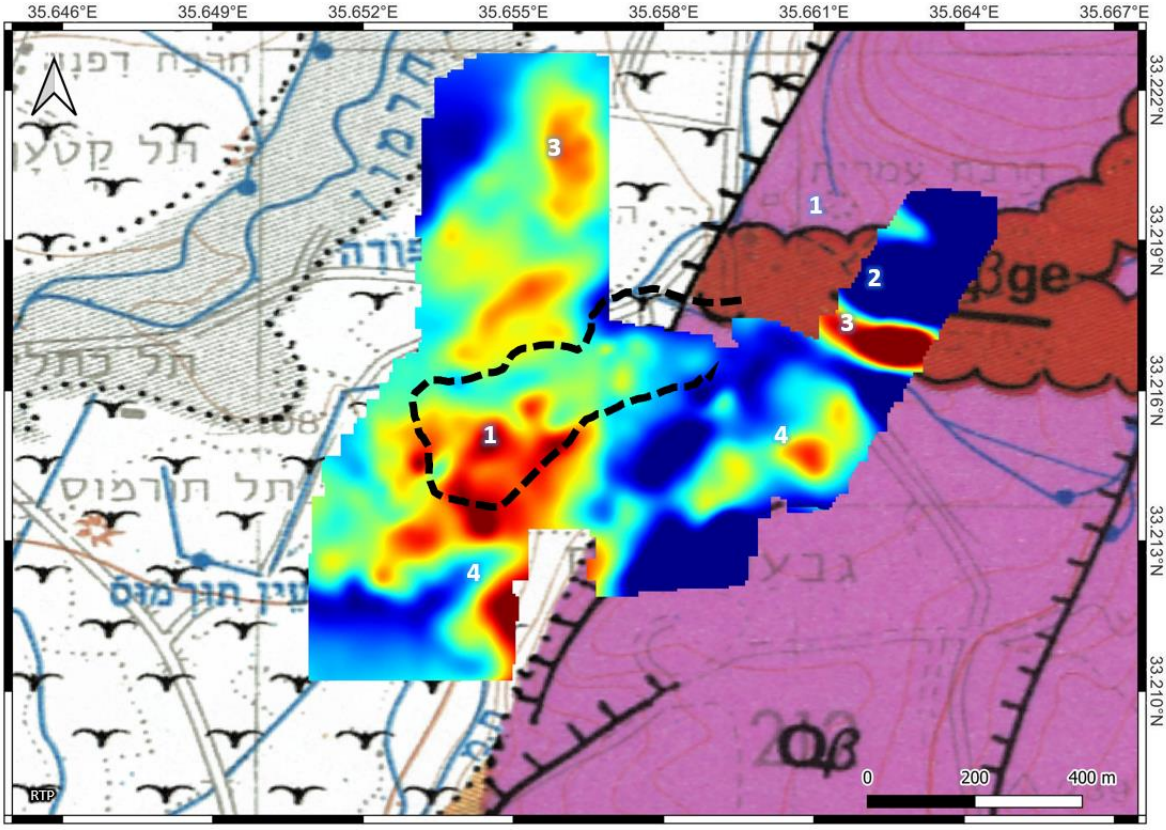

Figure 31 - Assessment of the Intra-basin continuation of the basaltic flows above the 25m RTP map and Mor's geological map (1987); Black dotted line – borders of the western part of flow F1 based on 50m aeromagnetic map

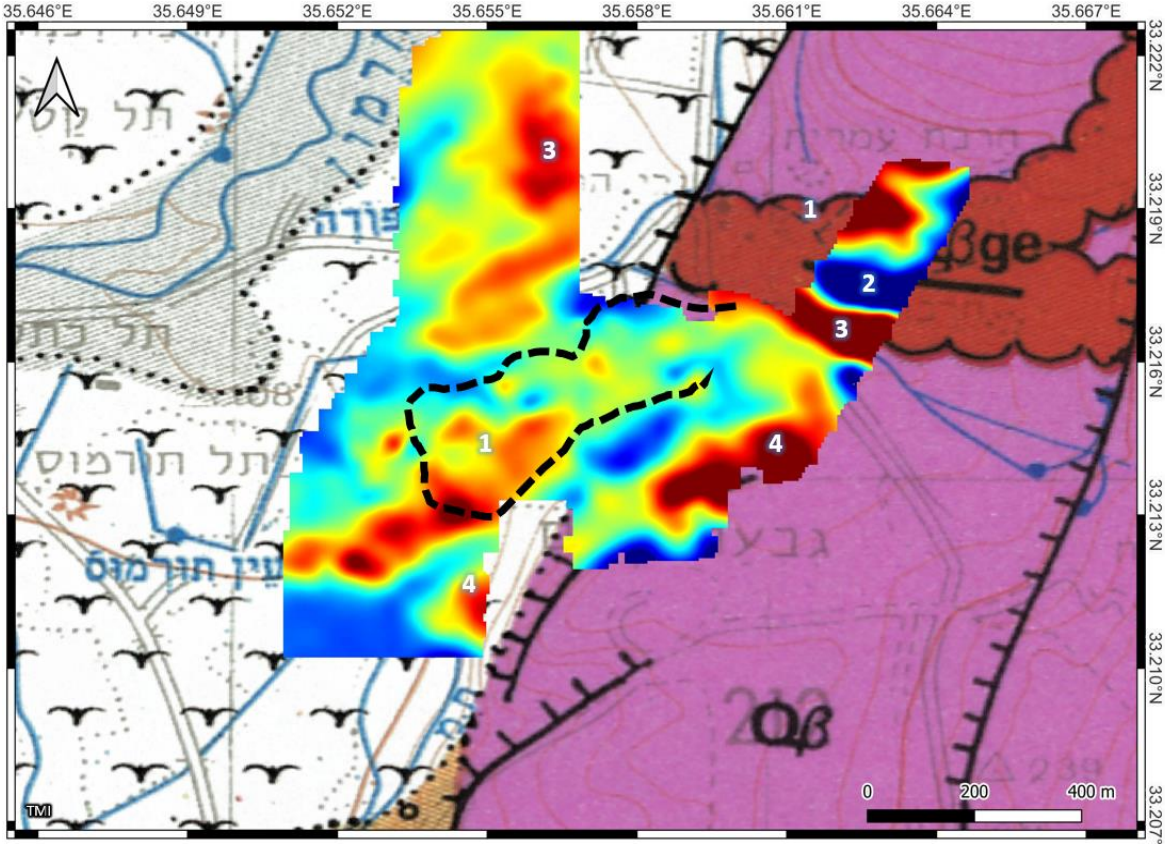

Figure 32 –Assessment of the Intra-basin continuation of the basaltic flows above the 25m TMI map and Mor's geological map (1987); Black dotted line – borders of the western part of flow number 1 based on 50m aeromagnetic map

4.2.3 Comparison with previous Ground surveys

Ground magnetic surveys were conducted as part of introductory courses in geophysics at the Hebrew University under the instruction of Amotz Agnon with Benjamin Medvedev (Kohn & Hassul, 2012; Paldor & Ziskind, 2013; Schechter & Bronstein, 2012). The data were collected using a GEM-19 OVERHAUSER magnetometer with a measurement frequency of 2 Hz. The raw data were processed using an Excel spreadsheet, and a magnetic anomaly map produced on a datum of approximately 41,180 nT. The survey results indicate that there is a strong anomaly southeast of the fault, and another strong anomaly from the east and northeast (Fig. 33, a,b,c) which appears at all heights .

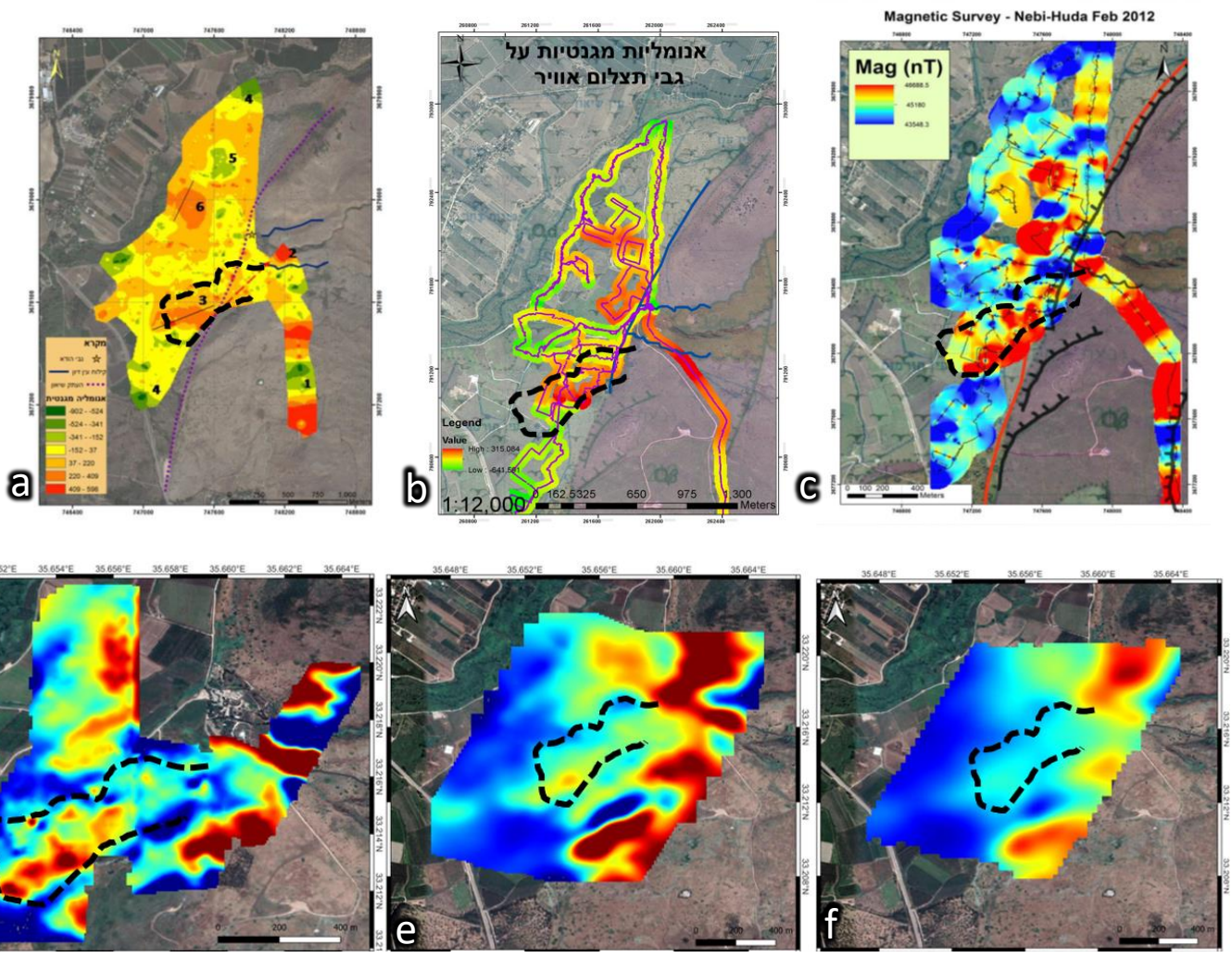

4.2.4 Upward continuation for depth assessment

To evaluate the depth of the Ein Zivan Flow (flow F1), an upward continuation of the 25 RTP map has been calculated (Fig.32). The main purpose is to elevate the data set to the height at which the assumed buried flow anomaly will be similar to the anomaly of the exposed source at 25m AGL (Fig. 34a)

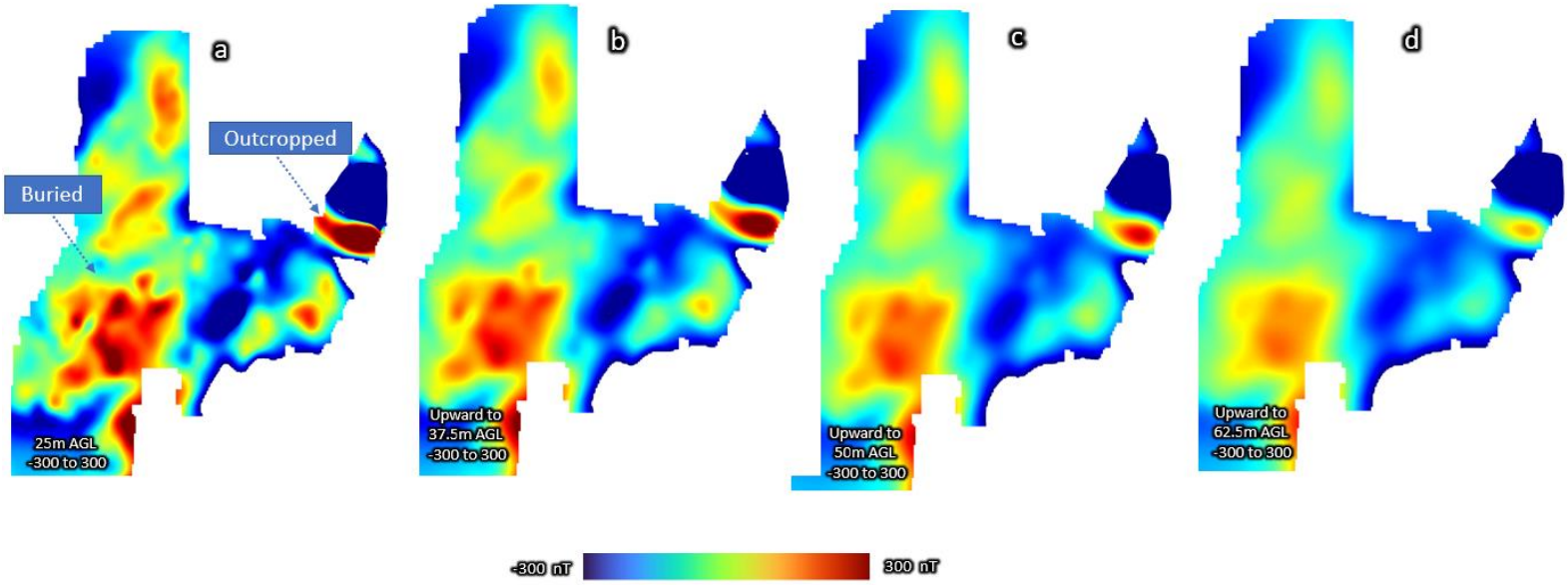

The top of the buried level seems to correlate with a height of 50m from the sensor (Fig. 34c), which means more than twenty-five meters under the surface. The strongest anomalies and the lower amplitude tops correlate with a 62.5m distance from the drone, which means a 37.5m depth (Fig. 34d). As the upward and downward transforms are mainly used for levelling different height data sets, and for the evaluation of distance to anomalies, such a calculation is essentially qualitative. Therefore, they should be considered as an additional indication that the anomalies we have identified are possibility, or indeed, buried basalts.

5. Summary and conclusions

This study presents a multi-scale high-resolution aeromagnetic UAV-based survey for detecting magmatic and tectonic features. A case study from the Hula Valley, one of the northern of the Dead Sea Fault's southern sector, was chosen.

The Nebi-Huda area is where the relationship between the Golan Formation flows, detached by the marginal Fault 'Azaz, and the margin of the Hula valley, is unclear. We surveyed HRAM at heights 100, 50, and 25 meters above the surface and processed the data using RTP and FVD transformations.

Oriented drill cores were also collected and analyzed fort paleomagnetic and AMS at three sites, representing the contact zone between the late-Pleistocene Ein Zivan Flows, and the mid-Pleistocene Yehudiyya-Dalwe Flows. In addition, the results were compared to three previous ground magnetic surveys.

The conclusions of the research are as follows:

- 'Azaz Fault appears distinctly across the scanned area and corresponds to the latest geological map in its location and strike.

- The results reveal a new main N-S limit, parallel to the known outcropping fault. This is interpreted as a buried fault system forming a probable stepping system.

- Three groups of second order faults are identified. These groups correlate to the regional trends of faulting. One of the groups strike NNE, paralleling the faults mapped tentatively by Mor (1987) adjacent to Givat-HaEm. Also, the groups resemble the typical phenomena of marginal faults by which zones of tension combine with zones of compression (Crider & Pollard, 1998; Matmon et al., 2010; Reches, 1987)

- In addition to the 'Azaz Fault, we interpreted a buried fault striking sub-parallel to the 'Azaz Fault.

- The buried faults seem to be part of the typical graded structure of marginal faults recognized by Politi (2011) who worked on seismic reflection sections recognized.

- The RTP maps show that all the visible flows, i.e., east of 'Azaz Fault, are of normal magnetization.

- The results of the AMS test show that the southern contact line between Ein Zivan and the unsorted basalts should be delineated, since the flow here differs from the one to the south. In addition, the results show that the flow direction corresponds to the same direction identified in the orthophoto. A similar trend is marked on the geological map of Mor (1987).

- The magnetic maps indicate the continuation of the Golan Flows within the subsiding Hula Valley; an upward continuation calculation presented an assumed minimal depth of 25-37.5 m for the top of the Ein Zivan flow, which is detached 200 to 300m south of the outcropping Ein Zivan flow, as mapped by Mor (1987).

- For a further investigation of the flow within the basin, we recommend drilling 50 m deep boreholes at the proposed locations marked in figures 29 and 30. As a second stage we recommend dating the basalts from drill cores and correlating them to the outcrops on the eastern side of the 'Azaz Fault.

6. Bibliography

Alken, P., Thébault, E., Beggan, C. D., Amit, H., Aubert, J., Baerenzung, J., Bondar, T. N., Brown, W. J., Califf, S., Chambodut, A., Chulliat, A., Cox, G. A., Finlay, C. C., Fournier, A., Gillet, N., Grayver, A., Hammer, M. D., Holschneider, M., Huder, L., … Zhou, B. (2021). International Geomagnetic Reference Field: the thirteenth generation. *Earth, Planets and Space*, *73*(1), 1–25. https://doi.org/10.1186/S40623-020-01288-X/FIGURES/5

Ambraseys, N. N. (1997). *The earthquake of 1 January 1837 in Southern Lebanon and N orthern Israel*. https://www.earth-prints.org/handle/2122/1595

Baranov, V., & Naudy, H. (1964). NUMERICAL CALCULATION of the FORMULA of REDUCTION to the MAGNETIC POLE. *Geophysics*, *29*(1), 67–79. https://doi.org/10.1190/1.1439334

Behar, N. A., Shaar, R., Tauxe, L., Asefaw, H., Ebert, Y., Heimann, A., Koppers, A. A. P., & Ron, H. (2019). *Paleomagnetism and Paleosecular Variations From the Plio-Pleistocene Golan Heights*. Geochemistry, Geophysics, Geosystems.

Blakely, R. J. (1996). Potential Theory in Gravity and Magnetic. In *Cambridge University Press*.

Calou, P., & Munschy, M. (2020). Airborne Magnetic Surveying with a Drone and Determination of the Total Magnetization of a Dipole. *IEEE Transactions on Magnetics*, *56*(6). https://doi.org/10.1109/TMAG.2020.2986988

Campbell, W. H. (2003). *Introduction to geomagnetic fields.* Cambridge University Press.

Channell, J. E. T. (2017). Cobb Mountain Subchron recorded at IODP Site U1306 (Eirik Drift, off SE Greenland). *Geophysical Journal International*, *209*(3), 1389–1397. https://doi.org/10.1093/GJI/GGX098

Crider, J. G., & Pollard, D. D. (1998). Fault linkage: Three-dimensional mechanical interaction between echelon normal faults. *Journal of Geophysical Research: Solid Earth*, *103*(10), 24373–24391. https://doi.org/10.1029/98JB01353

Cunningham, M. (2016). Aeromagnetic surveying with unmanned aircraft systems. *M.Sc. Thesis, Department of Earth Science, Carleton University, Ottawa, ON*, 1–156.

Cunningham, M., Samson, C., Wood, A., & Cook, I. (2018). Aeromagnetic Surveying with a Rotary-Wing Unmanned Aircraft System: A Case Study from a Zinc Deposit in Nash Creek, New Brunswick, Canada. *Pure and Applied Geophysics*, *175*(9), 3145–3158. https://doi.org/10.1007/S00024-017-1736-2/FIGURES/12

de Lépinay, J. M., Fréville, T., Gavazzi, B., Kiemes, B., Sanabria, L. M., Munschy, M., & Reiller, H. (2021). A versatile solution for high-quality UAV fluxgate magnetic acquisitions. *First Break*, *39*(8), 57–62. https://doi.org/10.3997/1365-2397.FB2021061/CITE/REFWORKS

Domzalski, W. (1967). *eromagnetic survey of Israel: interpretation. Institute for Petroleum Research and Geophysics*.

Elsasser. (1956, April 1). *Hydromagnetic Dynamo Theory*. REVIES OF MODERN PHYSICS. https://journals.aps.org/rmp/pdf/10.1103/RevModPhys.28.135

Eppelbaum, L. (2021). *System of Potential Geophysical Field Application in Archaeological Prospection 1 . Short description of the developed interpretation methodology in magnetic prospecting*. 1–43.

Eyal, Y. (1996). Stress field fluctuations along the Dead Sea rift since the middle Miocene. *Tectonics*, *15*(1), 157–170. https://doi.org/10.1029/95TC02619

Fassbinder, J. W. E. (2017). *Magnetometry for Archaeology*. 499–514. https://doi.org/10.1007/978-1-4020-4409-0_169

Feraud, G., York, D., Hall, C. M., Goren, N., & Schwarcz, H. P. (1983). 40Ar/39Ar age limit for an Acheulian site in Israel. *Nature 1983 304:5923*, *304*(5923), 263–265. https://doi.org/10.1038/304263a0

Frank, U., Schwab, M. J., & Negendank, J. F. W. (2002). A lacustrine record of paleomagnetic secular variations from Birkat Ram, Golan Heights (Israel) for the last 4400 years. *Physics of the Earth and Planetary Interiors*, *133*(1–4), 21–34. https://doi.org/10.1016/S0031-9201(02)00085-7

Frank, U., Schwab, M. J., Negendank, J. F. W., Frank, U., Schwab, M. J., & Negendank, J. F. W. (2003). Results of rock magnetic investigations and relative paleointensity determinations on lacustrine sediments from Birkat Ram, Golan Heights (Israel). *Journal of Geophysical Research: Solid Earth*, *108*(B8), 2379. https://doi.org/10.1029/2002JB002049

Freund, R. (1970). The shear along the Dead Sea rift. *Philosophical Transactions for the Royal Society of London.*, 107–130. https://www.jstor.org/stable/73612

Freund, R., Garfunkel, Z., Zak, I., Goldberg, M., Weissbrod, T., Derin, B., Bender, F., Wellings, F. E., & Girdler, R. W. (1970). A Discussion on the Structure and Evolution of the Red Sea and the Nature of the Red Sea, Gulf of Aden and Ethiopia Rift Junction. *Philosophical Transactions of the Royal Society of London. Series A, Mathematical and Physical Sciences*, *267*(1181), 107–130. https://www.jstor.org/stable/73612

Garfunkel, Z. (1981). Internal structure of the Dead Sea leaky transform (rift) in relation to plate kinematics. *Tectonophysics*, *80*(1–4), 81–108. https://doi.org/10.1016/0040-1951(81)90143-8

Gavazzi B, Le Maire P, Munschy M, & Dechamp A. (2016). Fluxgate vector magnetometers: a multi-sensor device for ground, UAV and airborne magnetic surveys. Leading Edge 35 (9): 795-797, 2016
DOI: 10.1190/tle35090795.1

Gavazzi, B., Alkhatib-Alkontar, R., Munschy, M., Colin, F., & Duvette, C. (2017). On the Use of Fluxgate 3-Axis Magnetometers in Archaeology: Application with a Multi-sensor Device on the Site of Qasr 'Allam in the Western Desert of Egypt. *Archaeological Prospection*, *24*(1), 59–73. https://doi.org/10.1002/ARP.1553

Gavazzi, B., le Maire, P., Mercier de Lépinay, J., Calou, P., & Munschy, M. (2019). Fluxgate three-component magnetometers for cost-effective ground, UAV and airborne magnetic surveys for industrial and academic geoscience applications and comparison

with current industrial standards through case studies. *Geomechanics for Energy and the Environment*, *20*, 100117. https://doi.org/10.1016/j.gete.2019.03.002

Ginzburg, A., & Ben-Avraham, Z. (1986). Structure of the sea of Galilee graben, Israel, from magnetic measurements. *Tectonophysics*, *126*(2–4), 153–164. https://doi.org/10.1016/0040-1951(86)90225-8

Gomez, F., Karam, G., Khawlie, M., McClusky, S., Vernant, P., Reilinger, R., Jaafar, R., Tabet, C., Khair, K., & Barazangi, M. (2007). Global Positioning System measurements of strain accumulation and slip transfer through the restraining bend along the Dead Sea fault system in Lebanon. *Geophysical Journal International*, *168*(3), 1021–1028. https://doi.org/10.1111/j.1365-246X.2006.03328.x

Gomez, F., Meghraoui, M., Darkal, A. N., Hijazi, F., Mouty, M., Suleiman, Y., Sbeinati, R., Darawcheh, R., Al-Ghazzi, R., & Barazangi, M. (2003). Holocene faulting and earthquake recurrence along the Serghaya branch of the Dead Sea fault system in Syria and Lebanon. *Geophys. J. Int*, *153*, 658–674. https://doi.org/10.1046/j.1365-246X.2003.01933.x

Gomez, F., Nemer, T., Tabet, C., Khawlie, M., Meghraoui, M., & Barazangi, M. (2007). Strain partitioning of active transpression within the Lebanese restraining bend of the Dead Sea Fault (Lebanon and SW Syria). *Geological Society Special Publication*, *290*, 285–303. https://doi.org/10.1144/290.10

Heimann, A. (1990). The Dead Sea rift and its margins. Development of Northern Israel in the Pliocene and Pleistocene.PhD Thesis. PhD Thesis Hebrew Univ [Hebrew university]. In *1990*. Google Scholar

Heimann, A., Eyal, M., & Eyal, Y. (1990). The evolution of Barahta rhomb-shaped graben, Mount Hermon, Dead Sea transform. *Tectonophysics*, *180*(1), 101–109. https://doi.org/10.1016/0040-1951(90)90375-I

Heimann, A., & Ron, H. (1987). Young faults in the Hula Pull-Apart Basin, central Dead Sea Transform. *Tectonophysics*, *141*(1–3), 117–124. https://doi.org/10.1016/0040-1951(87)90179-X

Heimann, A., & Steinitz, G. (1989). 40Ar/39Ar total gas ages of basalts from Notera #3 well, Hula Valley, Dead Sea Rift : Stratigraphic and tectonic implications. *Israel Journal of Earth-Sciences*, *38*(2–4), 173–184.

Heimann, A., Zilberman, E., Amit, R., & Frieslander, U. (2009). Northward migration of the southern diagonal fault of the Hula pull-apart basin, Dead Sea Transform, northern Israel. *Tectonophysics*, *476*(3–4), 496–511. https://doi.org/10.1016/j.tecto.2009.07.024

Heimann, Ariel & Ron, H. (1993). Geometric changes of plate boundaries along part of the northern Dead Sea Transform: Geochronologic and paleomagnetic evidence. *Tectonics*, *12*(2), 477–491. https://doi.org/10.1029/92TC01789

Hinze, W., von Frese, R.R.B, Saad, & A.H. (2013). *Gravity and Magnetic Exploration: Principles, Practices, and Applications - William J. Hinze, Ralph R. B. von Frese, R. Von Frese, Afif H. Saad*. https://books.google.com

Hrouda, F. (2007). Magnetic Susceptibility, Anisotropy. *Encyclopedia of Geomagnetism and Paleomagnetism*, 546–560. https://doi.org/10.1007/978-1-4020-4423-6_185

Hurwitz, S., Matmon, A., & Ron, H. , & H. A. (2000). "Deformation along the margins of the Dead Sea Transform: the Yahudia Block, Golan Heights." *Israel Journal of Earth Sciences*, *48*, 257–264. Google Scolar

Inbar, M., & Gilichinsky, M. (2009). *New Ar-Ar dates from lava flows and cinder cones in the Golan Heights—some geomorphic implications*. Israel Geological Society Meeting, Kfar Blum, Israel. Google scholar

Kohn, N., & Hassul, E. (2012). *פיזיקה של כדור "דוח סקר מגנטי בעמק החולה במסגרת הקורס הארץ."*

le Maire, P., Bertrand, L., Munschy, M., Diraison, M., & Géraud, Y. (2020). Aerial magnetic mapping with an unmanned aerial vehicle and a fluxgate magnetometer: a new method for rapid mapping and upscaling from the field to regional scale. *Geophysical Prospecting*, *68*(7), 2307–2319. https://doi.org/10.1111/1365-2478.12991

Lowrie, W. (2007). Lowrie, William, and Andreas Fichtner. Fundamentals of geophysics. Cambridge university press. In *Cambridge University Press*. Google Books

Malehmir, A., Dynesius, L., Paulusson, K., Paulusson, A., Johansson, H., Bastani, M., Wedmark, M., & Marsden, P. (2017). The potential of rotary-wing UAV-based magnetic surveys for mineral exploration: A case study from central Sweden. *Leading Edge*, *36*(7), 552–557. https://doi.org/10.1190/TLE36070552.1

Mankinen, E., Donnelly, J., Geology, C. G.-, & 1978, undefined. (1978). Geomagnetic polarity event recorded at 1.1 my BP on Cobb Mountain, Clear Lake volcanic field, California. *Geology*, *6.11*, 653–656. Google Scholar

Matmon, A., Katz, O., Shaar, R., Ron, H., Porat, N., & Agnon, A. (2010). Timing of relay ramp growth and normal fault linkage, Upper Galilee, northern Israel. *Tectonics*, *29*(2), 2016. https://doi.org/10.1029/2009TC002510

Mor, D. (1986). *The volcanism of the Golan Heights*. [publisher not identified].

Mor, D. (1993). A time-table for the levant volcanic province, according to K-Ar dating in the golan heights, Israel. *Journal of African Earth Sciences*, *16*(3), 223–234. https://doi.org/10.1016/0899-5362(93)90044-Q

Mor, D., MicheIson, H., Druckman, Y., Mimran, Y., Heimann, A., Goldberg, M., Sneh, A., Sneh, A., Druckman, Y., Mimran, akov, Heimann, A., Goldberg, M., Mor, D., & Michelson, H. (1997). *State of Israel The Ministry of National Infrastructures GeologicaI Survey of Israel NOTES ON THE GEOLOGY OF THE GOLAN HEIGHTS (Based on the 1:50,000 geological maps of Har Odem and Qazrin sheets*.

Mor, D., & Steinitz, G. (1983). "K-Ar age determination of the Cover Basalt surrounding the Sea of Galilee." *Isr. Geol. Soc. Annu. Meet.*, 62–64. https://scholar.google.com

Munschy, M., Boulanger, D., Ulrich, P., & Bouiflane, M. (2007). Magnetic mapping for the detection and characterization of UXO: Use of multi-sensor fluxgate 3-axis

magnetometers and methods of interpretation. *Journal of Applied Geophysics*, *61*(3–4), 168–183. https://doi.org/10.1016/j.jappgeo.2006.06.004

Nabighian, M. N., Grauch, V. J. S., Hansen, R. O., LaFehr, T. R., Li, Y., Peirce, J. W., Phillips, J. D., & Ruder, M. E. (2005). The historical development of the magnetic method in exploration. *Geophysics*, *70*(6). https://doi.org/10.1190/1.2133784/ASSET/IMAGES/LARGE/33ND_1_F6.JPEG

Nemer, T., & Meghraoui, M. (2006). Evidence of coseismic ruptures along the Roum fault (Lebanon): a possible source for the AD 1837 earthquake. *Journal of Structural Geology*, *28*(8), 1483–1495. https://doi.org/10.1016/J.JSG.2006.03.038

Nuriel, P., Weinberger, R., … A. K.-C.-, & 2017, undefined. (2017). The onset of the Dead Sea transform based on calcite age-strain analyses. *Geology*, *45*(7), 587–590. https://pubs.geoscienceworld.org/gsa/geology/article-abstract/45/7/587/207858

Paldor, & Ziskind. (2013). *Magnetic ground survey Nebi-Huda 2013*.

Pawlowski, R. S. (1995). Preferential continuation for potential-field anomaly enhancement. *Geophysics*, *60*(2), 390–398. https://doi.org/10.1190/1.1443775

Politi, M. (2011). *Transformation of terrestrial transform within a basin - evidence Ground subsidence in the Hula Valley*.

Politi, M., & Agnon, A. (2009). The Dead Sea Rift at The Hula Basin - An Example of Active Continental Transform Branching. *AGUFM*, *2009*, T54C-04. https://ui.adsabs.harvard.edu/abs/2009AGUFM.T54C..04P/abstract

Ravat, D. (2007). Upward And Downward Continuation. *Encyclopedia of Geomagnetism and Paleomagnetism*, 974–976. https://doi.org/10.1007/978-1-4020-4423-6_311

Reches, Z. (1987). Determination of the tectonic stress tensor from slip along faults that obey the Coulomb yield condition. *Tectonics*, *6*(6), 849–861. https://doi.org/10.1029/TC006I006P00849

Reilinger, R., McClusky, S., Vernant, P., Lawrence, S., Ergintav, S., Cakmak, R., Ozener, H., Kadirov, F., Guliev, I., Stepanyan, R., Nadariya, M., Hahubia, G., Mahmoud, S., Sakr, K., ArRajehi, A., Paradissis, D., Al-Aydrus, A., Prilepin, M., Guseva, T., … Karam, G. (2006). GPS constraints on continental deformation in the Africa-Arabia-Eurasia continental collision zone and implications for the dynamics of plate interactions. *Journal of Geophysical Research: Solid Earth*, *111*(5). https://doi.org/10.1029/2005JB004051

Ron, H., Freund, R., Garfunkel, Z., & Nur, A. (1984). Block rotation by strike-slip faulting: Structural and paleomagnetic evidence. *Journal of Geophysical Research: Solid Earth*, *89*(B7), 6256–6270. https://doi.org/10.1029/JB089IB07P06256

Rybakov, M., Fleischer, L., & ten Brink, U. (2003). The Hula Valley subsurface structure inferred from gravity data. *Israel Journal of Earth Sciences*, *52*(3–4), 113–122. https://doi.org/10.1560/WF6V-4BVG-GXQM-PKVR

Rybakov, M., Goldshmidt, V., Hall, J. K., Ben-Avraham, Z., & Lazar, M. (2011). New insights into the sources of magnetic anomalies in the Levant. *Russian Geology and Geophysics*, *52*(4), 377–397. https://doi.org/10.1016/J.RGG.2011.03.001

Rybakov, M., Goldshmidt, V., Hall, J. K., Ben-Avraham, Z., Lazar, M., Zilberman, E., Amit, R., Heimann, A., Porat, N., Mor, D., ten Brink, U. S., Rybakov, M., Al-Zoubi, A. S., Rotstein, Y., Segev, A., Rybakov, M., Heimann, A., Ron, H., Gomez, F., … Politi, M. (2003). Geology of the Metulla quadrangle, northern Israel: Implications for the offset along the Dead Sea Rift. *Tectonophysics*, *52*(1–4), 1–13. https://doi.org/10.1560/1G3J-NX0H-KBL3-RUY9

Rybakov, M., Goldshmidt, V., & Rotstein, Y. (1997). New regional gravity and magnetic maps of the Levant. In *GEOPHYSICAL RESEARCH LETTERS* (Vol. 24, Issue 1). https://doi.org/10.1029/96GL03617

Sadeh, M., Hamiel, Y., Ziv, A., Bock, Y., Fang, P., & Wdowinski, S. (2012). Crustal deformation along the Dead Sea Transform and the Carmel Fault inferred from 12 years of GPS measurements. *Journal of Geophysical Research: Solid Earth*, *117*(B8), 8410. https://doi.org/10.1029/2012JB009241

Sagy, A., Reches, Z., & Agnon, A. (2003). Hierarchic three-dimensional structure and slip partitioning in the western Dead Sea pull-apart. *Tectonics*, *22*(1). https://doi.org/10.1029/2001TC001323

Schattner, U., Segev, A., Mikhailov, V., Rybakov, M., & Lyakhovsky, V. (2019). Magnetic Signature of the Kinneret–Kinarot Tectonic Basin Along the Dead Sea Transform, Northern Israel. *Pure and Applied Geophysics*, *176*(10), 4383–4399. https://doi.org/10.1007/S00024-019-02211-6/FIGURES/10

Schattner, U., Segev, A., Mikhailov, V., Rybakov, M., & Lyakhovsky, V. (2022). Detailed Regional Magnetic Mapping on a Bike, A Case Study from Northern Israel. *Pure and Applied Geophysics*. https://doi.org/10.1007/s00024-022-03100-1

Schattner, U., & Weinberger, R. (2008). A mid-Pleistocene deformation transition in the Hula basin, northern Israel: Implications for the tectonic evolution of the Dead Sea Fault. *Geochemistry, Geophysics, Geosystems*, *9*(7).

Schechter, T., & Bronstein, N. (2012). *נבי הודא, ח מסכם של סקר מגנטי"דו*.

Segev, A., & Rybakov, M. (2011). History of faulting and magmatism in the Galilee (Israel) and across the Levant continental margin inferred from potential field data. *Journal of Geodynamics*, *51*(4), 264–284. https://doi.org/10.1016/J.JOG.2010.10.001

Shaanan, U., Porat, N., Navon, O., Weinberger, R., Calvert, A., & Weinstein, Y. (2011). OSL dating of a Pleistocene maar: Birket Ram, the Golan heights. *Journal of Volcanology and Geothermal Research*, *201*(1–4), 397–403. https://doi.org/10.1016/j.jvolgeores.2010.06.007

Sneh, A., & Weinberger, R. (2003). Geology of the Metulla quadrangle, northern Israel: Implications for the offset along the Dead Sea Rift. *Isr. J. Earth Sci*, *52*, 123–138.

Tauxe, L. (2002). Paleomagnetic Principles and Practice. In *2002*. https://books.google.com

Tauxe, L., Asefaw, H., Behar, N. A., Koppers, A. A. P., & Shaar, R. (2022). *Paleointensity Estimates from the Pleistocene of Northern Israel: Implications for hemispheric asymmetry in the time averaged field*. https://doi.org/10.1002/ESSOAR.10511070.1

Telford, W., Telford, W., Geldart, L., & Sheriff, R. (1990). Applied geophysics. In *1990*. Cambridge university press. https://books.google.com

ten Brink, U. S., Rybakov, M., Al-Zoubi, A. S., Rotstein, Y., Brink, U. S., Rybakov, M., Al-Zoubi, A. S., & Rotstein, Y. (2007). Magnetic character of a large continental transform: An aeromagnetic survey of the Dead Sea Fault. *Geochemistry, Geophysics, Geosystems*, *8*(7), 7005. https://doi.org/10.1029/2007GC001582

Weinstein, Y., Navon, O., Altherr, R., & Stein, M. (2006). *The Role of Lithospheric Mantle Heterogeneity in the Generation of Plio-Pleistocene Alkali Basaltic Suites from NW Harrat Ash Shaam (Israel)*. https://doi.org/10.1093/petrology/egl003

Weinstein, Y., Nuriel, P., Inbar, M., Jicha, B. R., & Weinberger, R. (2020). Impact of the Dead Sea Transform Kinematics on Adjacent Volcanic Activity. *Tectonics*, *39*(1), e2019TC005645. https://doi.org/10.1029/2019TC005645

Weinstein, Y., Weinberger, R., & Calvert, A. (2013). High-resolution 40Ar/39Ar study of Mount Avital, northern Golan: Reconstructing the interaction between volcanism and a drainage system and their impact on eruptive styles. *Bulletin of Volcanology*, *75*(5), 1–12. https://doi.org/10.1007/S00445-013-0712-7/TABLES/1

Zilberman, E., Amit, R., Heimann, A., & Porat, N. (2000). Changes in Holocene paleoseismic activity in the Hula pull-apart basin, Dead Sea Rift, northern Israel. *Tectonophysics*, *321*(2), 237–252. https://doi.org/10.1016/S0040-1951(00)00035-4

7. Appendix

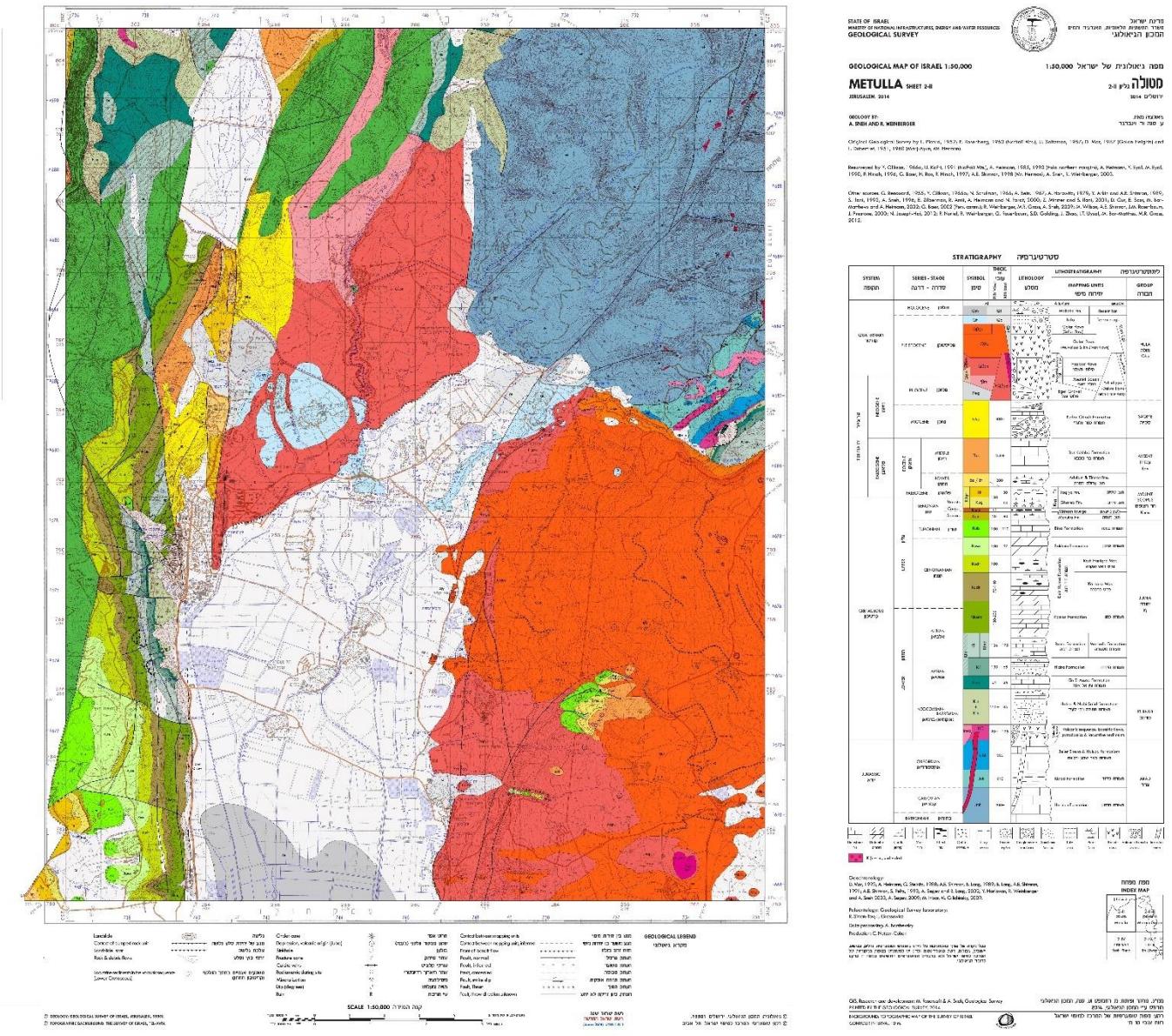

Figure 35 - Sneh and Weinberger Geological map (2014)

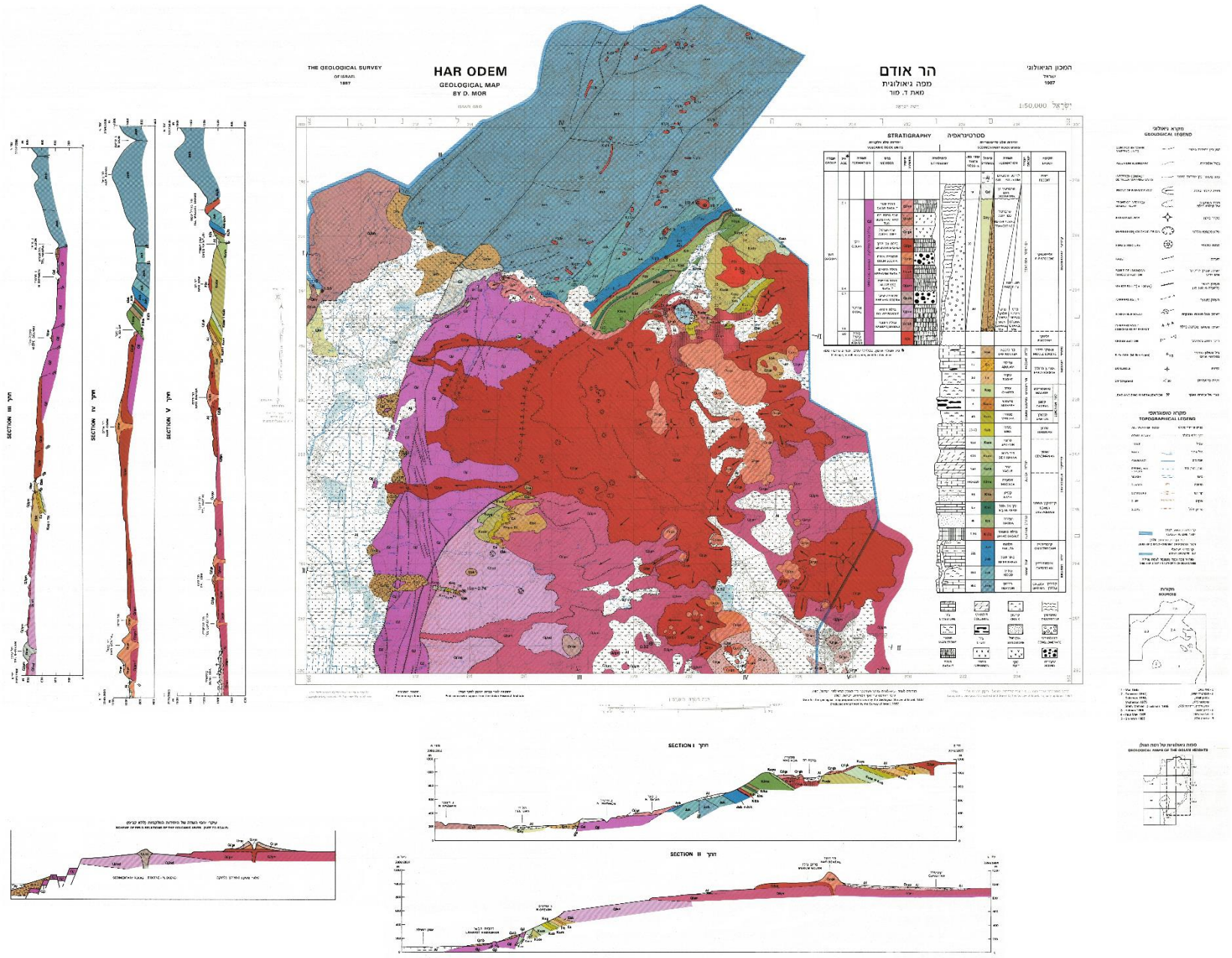

Figure 36 - Mor's 1:50,000 geological map (1987)

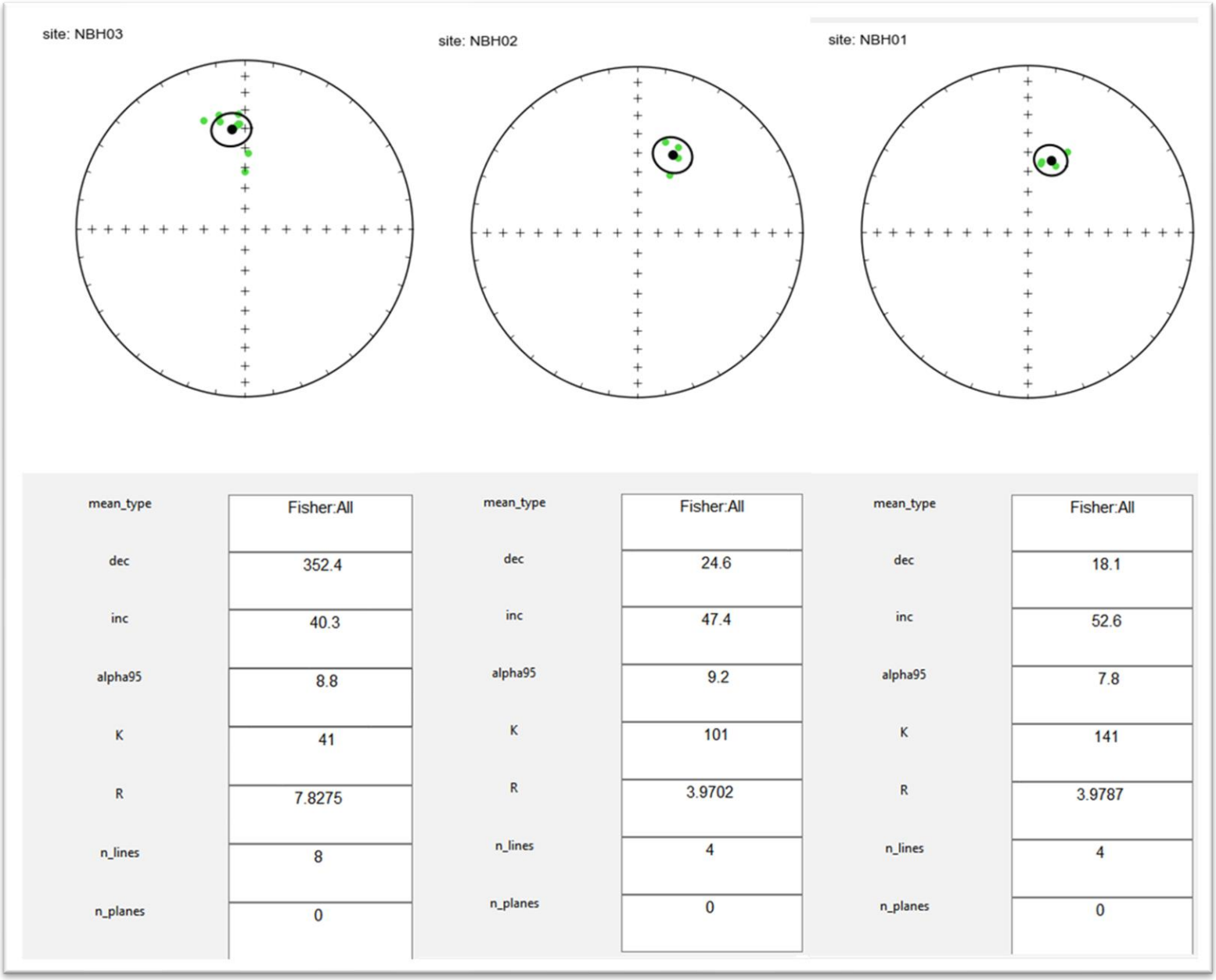

mean_type	Fisher:All
dec	352.4
inc	40.3
alpha95	8.8
K	41
R	7.8275
n_lines	8
n_planes	0

mean_type	Fisher:All
dec	24.6
inc	47.4
alpha95	9.2
K	101
R	3.9702
n_lines	4
n_planes	0

mean_type	Fisher:All
dec	18.1
inc	52.6
alpha95	7.8
K	141
R	3.9787
n_lines	4
n_planes	0

Figure 37 - Fisher statistics of the AMS